

## Black hole pulsars and monster shocks as outcomes of black hole–neutron star mergers

YOONSOO KIM,<sup>1,2</sup> ELIAS R. MOST,<sup>1,3</sup> ANDREI M. BELOBORODOV,<sup>4,5</sup> AND BART RIPPERDA<sup>6,7,8,9</sup>

<sup>1</sup>TAPIR, Mailcode 350-17, California Institute of Technology, Pasadena, CA 91125, USA

<sup>2</sup>Department of Physics, California Institute of Technology, Pasadena, CA 91125, USA

<sup>3</sup>Walter Burke Institute for Theoretical Physics, California Institute of Technology, Pasadena, CA 91125, USA

<sup>4</sup>Physics Department and Columbia Astrophysics Laboratory, Columbia University, 538 West 120th Street New York, NY 10027, USA

<sup>5</sup>Max Planck Institute for Astrophysics, Karl-Schwarzschild-Str. 1, 85741 Garching, Germany

<sup>6</sup>Canadian Institute for Theoretical Astrophysics, 60 St. George St, Toronto, ON M5S 3H8, Canada

<sup>7</sup>Department of Physics, University of Toronto, 60 St. George St, Toronto, ON M5S 1A7, Canada

<sup>8</sup>David A. Dunlap Department of Astronomy & Astrophysics, University of Toronto, Toronto, ON M5S 3H4, Canada

<sup>9</sup>Perimeter Institute for Theoretical Physics, 31 Caroline St. North, Waterloo, ON N2L 2Y5, Canada

### ABSTRACT

The merger of a black hole (BH) and a neutron star (NS) in most cases is expected to leave no material around the remnant BH; therefore, such events are often considered as sources of gravitational waves without electromagnetic counterparts. However, a bright counterpart can emerge if the NS is strongly magnetized, as its external magnetosphere can experience radiative shocks and magnetic reconnection during/after the merger. We use magnetohydrodynamic simulations in the dynamical spacetime of a merging BH–NS binary to investigate its magnetospheric dynamics. We find that compressive waves excited in the magnetosphere develop into monster shocks as they propagate outward. After swallowing the NS, the BH acquires a magnetosphere that quickly evolves into a split monopole configuration and then undergoes an exponential decay (balding), enabled by magnetic reconnection and also assisted by the ring-down of the remnant BH. This spinning BH drags the split monopole into rotation, forming a transient pulsar-like state. It emits a striped wind if the swallowed magnetic dipole moment is inclined to the spin axis. We predict two types of transients from this scenario: (1) a fast radio burst emitted by the shocks as they expand to large radii and (2) an X/ $\gamma$ -ray burst emitted by the  $e^\pm$  outflow heated by magnetic dissipation.

*Keywords:* Black holes (162), General relativity (641), Gamma-ray bursts (629), High energy astrophysics (739), Neutron stars (1108), Plasma astrophysics (1261), X-ray bursts (1814), Radio bursts (1339), Transient sources (1851), Relativistic binary stars (1386)

### 1. INTRODUCTION

Merging black hole (BH)–neutron star (NS) binaries are promising sources of gravitational waves (GWs) (see, e.g. Abbott et al. 2021, 2020; Abac et al. 2024, for recent detections). Depending on the mass ratio of the system and spin of the black hole, near-equal mass systems can feature tidal disruption of the neutron star during merger, leading to dynamical mass ejection and

the formation of a massive disk (Foucart 2012; Foucart et al. 2018). These can power electromagnetic (EM) counterparts such as kilonova afterglows (Lattimer & Schramm 1974; Li & Paczynski 1998; Tanaka et al. 2014; Kawaguchi et al. 2016; Fernández et al. 2017; Metzger 2020; Gottlieb et al. 2023a; Kawaguchi et al. 2024) and gamma-ray bursts (GRBs) (Janka et al. 1999; Etienne et al. 2012a,b; Paschalidis et al. 2015; Shapiro 2017; Ruiz et al. 2018; Hayashi et al. 2022; Gottlieb et al. 2023b; Martineau et al. 2024). However, the high mass ratio typical of such systems (Abbott et al. 2021; Abac et al. 2024) would likely result in a non-disruptive merger, leaving little or no matter surrounding the remnant BH

ykim7@caltech.edu

emost@caltech.edu

(Foucart 2012; Foucart et al. 2018). Most BH–NS mergers are expected to fall in this latter category and be EM-quiet (Fragione 2021; Biscoveanu et al. 2022), supported by the absence of EM counterparts to previous detections (e.g. Anand et al. 2021).

On the other hand, neutron stars can be equipped with strong exterior magnetic fields, leading to potential EM counterparts from magnetospheric interactions with their binary companion. Previously studied scenarios can be broadly split into two groups. Transients before merger (precursors) can be produced through magnetospheric interactions (McWilliams & Levin 2011; Lai 2012; Piro 2012; Paschalidis et al. 2013; Carrasco et al. 2019, 2021) including flares (Most & Philippov 2023; Beloborodov 2021), or through gravitationally driven resonances in the neutron star such as crustal shattering (Tsang et al. 2012; Penner et al. 2012; Most et al. 2024a). Potential transients at merger (concurrent EM counterpart) have been attributed to either a net electric charge of the black hole (Levin et al. 2018; Zhang 2019; Dai 2019; Pan & Yang 2019; Zhong et al. 2019), or magnetic flux shedding during the merger process (D’Orazio & Levin 2013; Mingarelli et al. 2015; D’Orazio et al. 2016; East et al. 2021).

Predicting magnetospheric dynamics of the merger is intrinsically complicated by various competing processes, some of which can be inferred from previous numerical studies of a NS gravitationally collapsing into a BH. In this related scenario, part of the magnetic field is immediately shed during the collapse (Baumgarte & Shapiro 2003; Lehner et al. 2012; Palenzuela 2013; Most et al. 2018). In the absence of resistive dissipation, the resulting BH can in principle acquire a net electric charge (Nathanail et al. 2017). However, pair-production in realistic environments will lead to an active magnetosphere supporting magnetic flux decay (balding) of the BH (Lyutikov & McKinney 2011; Bransgrove et al. 2021; Selvi et al. 2024). On a technical level, most of the studies in numerical relativity have made use of the force-free electrodynamics or vacuum approaches to study magnetospheric dynamics. Compared to magnetohydrodynamic (MHD) approaches explicitly tracking matter dynamics, these crucially miss out the formation of monster radiative shocks from fast magnetosonic waves (Beloborodov 2023) as was recently demonstrated by Most et al. (2024a), which could be responsible for some of the high-energy emission in this process.

Here, we present general relativistic (GR-)MHD simulations in full numerical relativity of a merging BH–NS binary, in which the NS is swallowed whole. While BH–NS merger simulations in GRMHD have become common (e.g., Chawla et al. 2010; Etienne et al. 2012a,b;

Kiuchi et al. 2015; Ruiz et al. 2018, 2020; Most et al. 2021; Hayashi et al. 2022, 2023; Izquierdo et al. 2024, tracking the magnetospheric evolution requires special flooring techniques (Tchekhovskoy et al. 2013; Parfrey & Tchekhovskoy 2017). We employ such a sophisticated MHD strategy to track the evolution of magnetosphere throughout inspiral and merger. Our simulations identify novel types of shock-powered and reconnection-driven transients from a BH–NS merger. Specifically, we show that monster shocks are formed during the final phase of the inspiral, which can primarily source X-ray and radio bursts. In the post-merger phase, we find that the magnetosphere of the remnant BH re-arranges into a short-lived *black hole pulsar* state (Selvi et al. 2024), capable of powering X-ray transients that may last for several milliseconds.

We describe the simulation setup and the configuration of the binary in Sec. 2. This is followed by detailed discussions of two new transients from non-disrupting BH–NS mergers. First, we present the formation of monster shocks in Sec. 3. Next, we provide a detailed analysis of the black hole pulsar state that our simulations reveal in Sec. 4. We discuss the properties of the expected EM emissions in Sec. 5. Finally, we conclude by summarizing our findings in Sec. 6. Unless otherwise stated, we adopt Gaussian units with  $c = G = 1$  throughout this paper.

## 2. METHODS

We track the time evolution of a BH–NS binary as well as the common binary magnetosphere using ideal GRMHD for dynamical spacetimes (Duez et al. 2005). To this end, we need to specify both initial conditions and evolution parameters.

We use the Kadath/FUKA (Papenfort et al. 2021; Grandclement 2010) initial data framework to construct BH–NS initial data in extended conformal thin sandwich (XCTS) form (Grandclement 2006; Taniguchi et al. 2007, 2008; Foucart et al. 2008; Tacik et al. 2016). In order to ensure that the NS is fully swallowed at merger,<sup>1</sup> we adopt a non-spinning NS with mass  $M_{\text{NS}} = 1.4M_{\odot}$  using the APR4 equation of state (Akmal et al. 1998), and a BH with mass  $M_{\text{BH}} = 8.0M_{\odot}$  and dimensionless spin  $a = 0.3$  aligned with the orbital axis ( $\hat{z}$ ). The initial orbital separation of the binary is 60km, resulting in  $\sim 1.5$  orbits before the merger. The neutron star is initially magnetized with a dipolar field with a strength  $|B_*| = 1.9 \times 10^{16}$  G at the magnetic poles on the surface. The precise value of the magnetic field is unimportant

<sup>1</sup> See Foucart (2012); Foucart et al. (2018) for the allowed parameter space of a non-disrupting BH–NS merger.

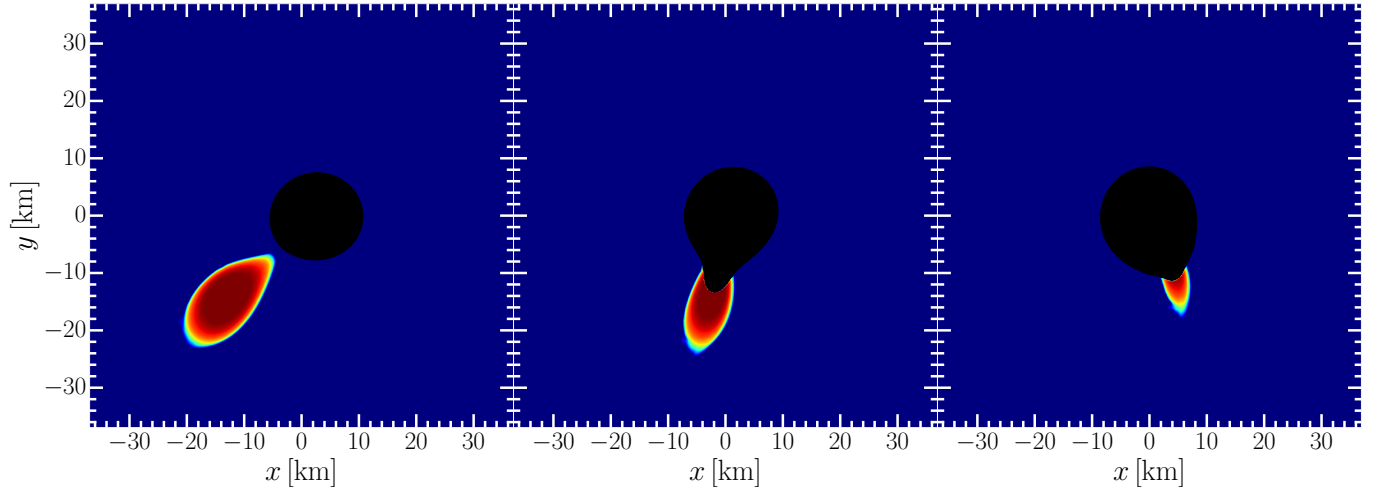


**Figure 1.** Merger of the BH–NS binary in our simulations, where the neutron star is swallowed whole. The entire process shown in this figure happens in less than one millisecond.

for the magnetospheric dynamics we study, since we fix the properties of the magnetosphere in terms of dimensionless quantities such as magnetization  $\sigma = b^2/\rho$ , and plasma  $\beta = 2P/b^2$ , where  $b^2$  is the magnetic energy density,  $\rho$  the rest-mass density and  $P$  the pressure. This allows us to rescale the resulting magnetospheric dynamics to arbitrary magnetic field strength. However, for purely numerical reasons we have found that using a stronger field strength eases the transition to a near force-free magnetosphere near the stellar surface in the inspiral computationally. Nevertheless, the chosen strength of the magnetic field hardly impacts the bulk dynamics of the NS (the plasma beta parameter is around  $\beta \sim 10^3$  inside the NS during the inspiral). We simulate three models with an initial inclination between the magnetic dipole moment and the orbital axis  $\theta_B = 0^\circ, 30^\circ$ , and  $60^\circ$ . The initial NS magnetic field is inclined toward the companion BH at  $t = 0$ .

Dynamical evolutions are performed with the Einstein Toolkit framework (Loffler et al. 2012), using the Frankfurt/IllinoisGRMHD (FIL) (Most et al. 2019; Etienne et al. 2015) code for solving the ideal GRMHD equations in a dynamical spacetime. The spacetime is evolved using FIL’s numerical relativity solver, which implements the Z4c equations (Bernuzzi & Hilditch 2010; Hilditch et al. 2013) in moving puncture gauge (Alcubierre et al. 2003) using a fourth-order finite-difference discretization (Zlochower et al. 2005). The ideal GRMHD equations are solved using the ECHO scheme (Del Zanna et al. 2007) with upwind constraint transport (Londrillo & Del Zanna 2004). Similar to our previous work (Most et al. 2024a), the fourth-order derivative corrector in the ECHO scheme showed less robust behavior at strongly magnetized shockfronts, and we have disabled it in our runs. A key feature of our

simulations is the ability to track the common magnetospheric dynamics in full MHD as opposed to vacuum or force-free electrodynamics. While several studies have evolved magnetic fields in the exterior region in the context of BH–NS mergers (Paschalidis et al. 2015; Ruiz et al. 2018, 2020), reproducing correct (near-) force-free magnetospheric dynamics within the MHD formulation requires the use of robust primitive inversion schemes (Kastaun et al. 2021) and special flooring techniques (Tchekhovskoy et al. 2013; Parfrey & Tchekhovskoy 2017), unlike floors commonly used in numerical relativity simulations (e.g. Poudel et al. 2020). A detailed prescription of the floors we use here is provided in Most et al. (2024a). It is precisely this flooring scheme that allows us to correctly capture and uncover the transients we present in this study. Similar to Most et al. (2024a), we have supplemented the high-density cold equation of state used in the initial data with a thermal equation of state,  $P_{\text{th}} = \rho\epsilon$ , which primarily governs the magnetospheric dynamics. Here  $P_{\text{th}}$  is the thermal pressure, and  $\epsilon$  the specific internal energy. We use a three-dimensional Cartesian grid with eight levels of nested moving mesh refinement (Schnetter et al. 2004). The coarsest grid extends to  $[-3025\text{km}, 3025\text{km}]^3$  and the finest resolution is 168 m. The finest grid level consists of two patches covering  $2\text{--}3\times$  the size of the NS as well as of the BH, being centered to and tracking each of them.

A detailed description of the initial evolution of non-disruptive BH–NS mergers can be found elsewhere (see e.g. Kyutoku et al. 2021, for a recent review). Since the magnetospheric transients in our simulations are mainly driven during and after the merger, we briefly depict the merger process in Figure 1, which highlights the high degree of spatial asymmetry present in the process, and

consequently, the need for full numerical relativity not only for the spacetime evolution but particularly to correctly determine the geometry of magnetic field in the post-merger phase.

### 3. MONSTER SHOCK

The initially dipolar magnetosphere of the NS is sheared in the vicinity of the BH before and during merger. This perturbation will launch waves into the magnetosphere, which will either be transverse (Alfvén) wave propagating along the magnetic field, or be a compressional (fast magnetosonic) wave. In a dipole background field, the compressional waves are expected from any non-toroidal perturbation in the magnetosphere, as happens during the merger.

Propagation of fast magnetosonic waves to larger radii  $r$  is not affected by the background field as long as their wave amplitude  $E = \delta B \propto r^{-1}$  is much smaller than the background dipole field  $B_{\text{bg}} \propto r^{-3}$ . With increasing  $r$ , this condition becomes broken,  $B^2 - E^2$  approaches zero, and the plasma drift speed in the wave approaches the speed of light.<sup>2</sup> will only happen efficiently on closed field lines inside the light cylinder, in turn requiring a minimum amplitude of the perturbation (see, e.g., [Most et al. \(2024b\)](#) for a discussion in the context of non-linear steepening of Alfvén waves). Recent analytical ([Beloborodov 2023](#)) and numerical ([Chen et al. 2022](#); [Vanthieghem & Levinson 2025](#)) works have demonstrated that this leads to the formation of *monster shocks* (see also [Lyubarsky \(2003\)](#) for earlier work). In particular, in the equatorial plane of the magnetic dipole, the shock appears when  $\delta B \approx B_{\text{bg}}/2$ , which implies  $B^2 - E^2$  touching zero at the trough of the compressional wave. Near this point, the plasma develops a characteristic negative velocity  $v^r < 0$ , which leads to shock formation in front of the crest of the wave. In practice, searching for zones with  $v_r < 0$  provides a simple way to identify regions of shock formation, in addition to detection of velocity jumps and localized heating spikes. A similar analysis was performed in [Most et al. \(2024a\)](#) to demonstrate shock formation in the magnetosphere of a collapsing magnetar.

In our simulations, the inspiral of the magnetized NS drives a continuous excitation of magnetosonic waves in the magnetosphere, peaking around the plunge of the NS into the BH. The final plunge of the NS injects a strong rarefaction mode into the surrounding magnetosphere as the NS bulk velocity is maximally radially inward at

the moment. In [Fig. 2](#), we show the excited magnetosphere about half an orbit before the plunge for aligned ( $\theta_B = 0^\circ$ ) magnetic axis. We find that the wave emitted during the plunge leads to the development of a large  $v^r < 0$  region characteristic of the monster shock, which we show in the top row of [Fig. 3](#). This phenomenology of a leading shock with surrounding weaker shocks resembles the results for the collapsing magnetar ([Most et al. 2024a](#)), and approximately agrees with the analytical prediction ([Beloborodov 2023](#), see [Fig. 7](#) therein).

The profile of  $\gamma v^r$  across the shock region is affected by deviations of  $B_{\text{bg}}$  from a pure dipole due to the orbital motion of the NS. As an additional validation, we have also confirmed that the regions with  $v^r < 0$  develop  $E^2 \approx B^2$  plateaus, corroborating that the observed feature is the monster shock.

We have also identified monster shocks for the inclined models. One such model with  $\theta_B = 60^\circ$  is shown in the bottom row of [Fig. 3](#). We caution that due to the misalignment between magnetic equator and orbital plane, the strongest part of the shock will appear off the shown  $yz$  plane, and the trough of the wave preceding the monster shock might not strongly exhibit  $v^r < 0$ . Yet, we can clearly identify a similar leading shock structure as in the aligned case.

### 4. TRANSIENT BLACK HOLE PULSAR

In this section, we present a detailed analysis of the evolution of the post-merger magnetosphere, defined as the region within the light sphere ( $r/c \leq t - t_{\text{merger}}$ ), with a special emphasis on the near-horizon dynamics. The merger remnant settles down to a Kerr BH with the mass  $M = 9.2M_\odot$  and the dimensionless spin  $a = 0.57$ . Relevant length and time scales are  $r_g \equiv GM/c^2 = 13.6\text{km}$  and  $r_g/c = 46\mu\text{s}$ , or equivalently 1 millisecond amounts to  $\sim 22r_g/c$ . The angular velocity of the outer event horizon is  $\Omega_H = ac/2r_+ = 3.43 \times 10^3\text{s}^{-1}$ , where  $r_+ = r_g(1 + \sqrt{1 - a^2}) \approx 25\text{km}$  is the outer horizon radius. While we will quote values measured from our simulation data in the following discussions, we caution that it is nontrivial to map our results (especially time scales) in a coordinate-independent manner to those obtained from other studies that used a fixed Kerr background, since our merger simulations are performed using dynamically evolved coordinates.

#### 4.1. Relaxation into a rotating split-monopole

The remnant BH is immersed in a dipole-like magnetic field shortly after the merger. Since black holes cannot support closed magnetic field lines ([MacDonald & Thorne 1982](#)), the dipole gets stretched out, with the magnetic field lines opening up near the magnetic equator. In consequence, the BH magnetosphere transitions

<sup>2</sup> Orbiting systems possess an orbital light cylinder,  $r_{\text{LC}} \sim 1/\Omega_{\text{orb}}$ , set by the orbital frequency  $\Omega_{\text{orb}}$ . Steepening or distortion of the waves induced by a decreasing  $B_{\text{bg}}$

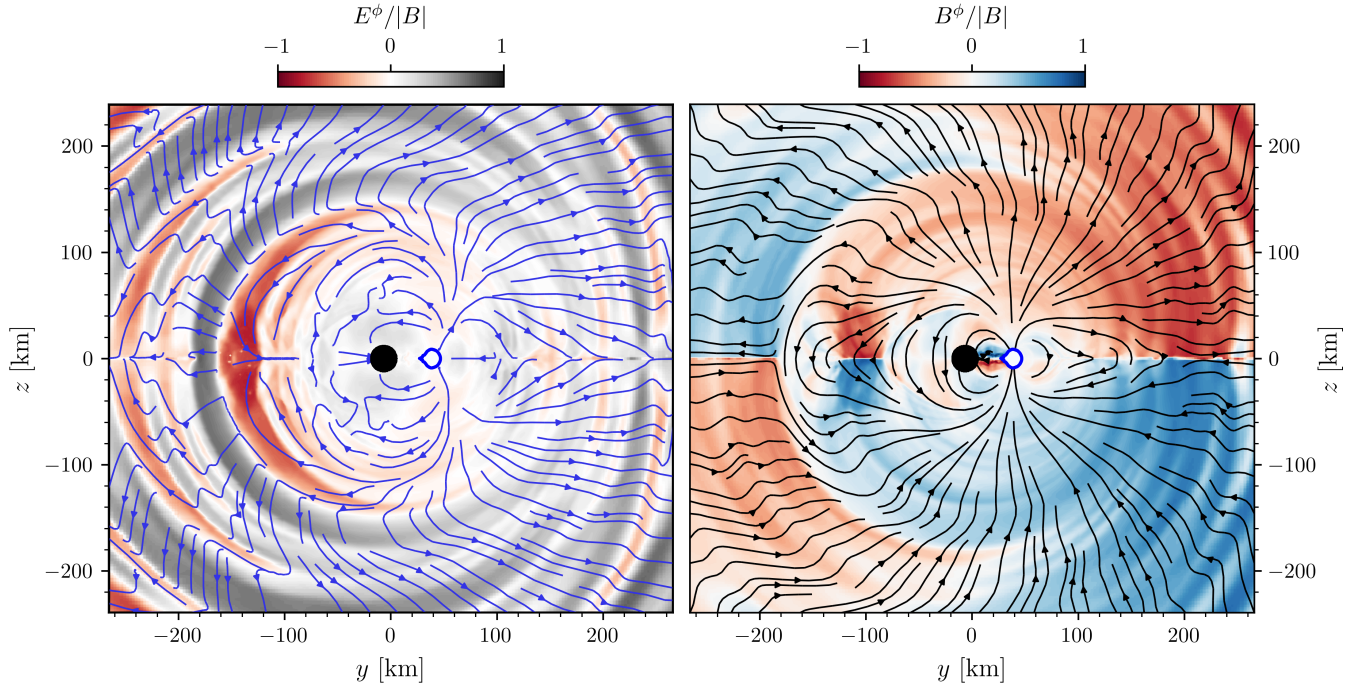


**Figure 2.** Poloidal structure (cut in the  $yz$  plane) of the perturbed magnetosphere of the BH–NS binary 0.9 ms before merger for the aligned ( $\theta_B = 0^\circ$ ) model. Fast magnetosonic waves have toroidal electric fields  $E^\phi$  (left), and Alfvén waves have toroidal magnetic perturbations  $\delta B^\phi$  (right). Streamlines show fluid velocity in the left panel and magnetic field lines in the right panel. The BH and NS are shown with a black and blue circle, respectively.

into a split-monopole topology (Komissarov 2004a), and begins to dissipate the magnetic field energy at the current sheet. The inclination of the split-monopole configuration depends on the initial inclination of the NS magnetic field. For all simulations, the topology of magnetic field lines transitions into a split-monopole over a timescale of 1 ms,<sup>3</sup> which is consistent with multiple light crossing times across the horizon ( $2r_+/c \approx 0.2$  ms).

The distribution of magnetic flux on the remnant BH is initially highly localized to the spot through which the NS plunged into (Fig. 1). Over the transition period to a split-monopole ( $t - t_{\text{merger}} \lesssim 1$  ms), the magnetic flux density on the BH horizon is redistributed, relaxing into a relatively uniform distribution by  $t - t_{\text{merger}} \approx 2$  ms. The upper panels of Fig. 4 show the post-merger magnetosphere at  $t - t_{\text{merger}} = 3.3$  ms for the aligned model ( $\theta_B = 0^\circ$ ), displaying an axisymmetric split-monopole magnetosphere centered on the BH. Magnetic energy of the magnetosphere is partially dissipated via reconnection in the equatorial current sheet, heating the plasma, as can be seen from the plot of  $P_{\text{th}}/\rho$  in Fig. 4.

<sup>3</sup> A similar reordering and collimation of the post-merger magnetic field may also have been observed in previous works (East et al. 2021).

The frame dragging of the remnant BH induces corotation of magnetic field lines and forms a rotating split-monopole. The angular velocity of the magnetic field lines in an axisymmetric force-free split-monopole magnetosphere around a Kerr BH is given as  $\Omega_F = a/8M$  to leading order in the spin (Komissarov 2004b; Armas et al. 2020). For arbitrary high spins,  $\Omega_F$  can be calculated either with a perturbative analytic expansion (e.g. Armas et al. 2020) or using an iterative numerical method (e.g. Contopoulos et al. 2013; Nathanail & Contopoulos 2014). The ratio  $\Omega_F/\Omega_H$ , which is 1/2 in the limit  $a \rightarrow 0$ , remains  $\lesssim 1\%$  different from 1/2 for the spin  $a \leq 0.7$  (e.g. see Figure 1 of Contopoulos et al. 2013). Therefore, in the case of our merger remnant BH with  $a = 0.57$ , we can safely assume  $\Omega_F/\Omega_H \simeq 0.5$ .

For the aligned ( $\theta_B = 0^\circ$ ) model, we measure the rotation angular velocity of magnetic field lines as

$$\Omega_F = \frac{-y(u^x/u^0) + x(u^y/u^0)}{\varpi^2}, \quad (1)$$

where  $u^\mu$  is the four-velocity of the plasma and  $\varpi = \sqrt{r^2 - z^2}$  is the (coordinate) cylindrical radius. This description is appropriate for the ideal MHD limit we consider. Fig. 5 shows the measured  $\Omega_F/\Omega_H$  over a spherical surface  $r = 2.4r_g$  encompassing the remnant

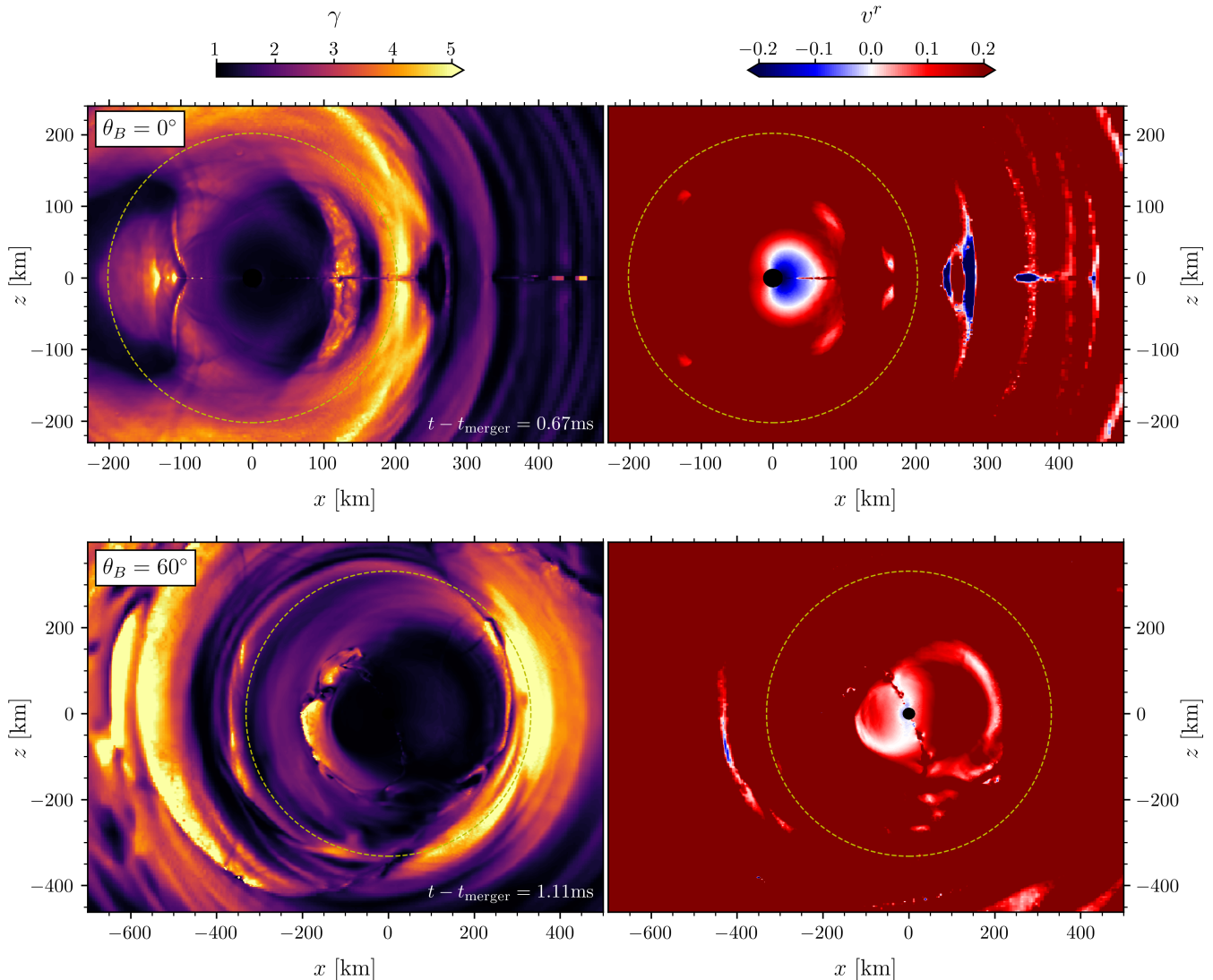


**Figure 3.** Monster shocks launched from BH-NS mergers. Shown here are the Lorentz factor (left panels) and the radial spatial velocity (right panels) on the meridional ( $xz$ ) plane. Dashed orange circles are light spheres with the radius  $r = c(t - t_{\text{merger}})$ . (Top) Simulation snapshot from the aligned model ( $\theta_B = 0^\circ$ ). A monster shock can be found near  $x \simeq 250\text{km}$ , with its characteristic feature of a plasma moving radially inward ( $v^r < 0$ ) preceding the shockfront. (Bottom) Inclined model  $\theta_B = 60^\circ$ . A similar feature can be seen near  $x \simeq -400\text{km}$ .

BH.<sup>4</sup> We observe that the rotation angular velocity of magnetic field lines converges to  $\Omega_H/2$  and the asymmetry present in its distribution is decayed out over time. In addition to the magnetic field morphology shown in Fig. 4, this provides solid evidence that the post-merger magnetosphere relaxes into a rotating split-monopole.

As naturally expected, for inclined magnetic field, the remnant BH settles down to a rotating, inclined split-monopole magnetosphere. The resulting global dynamics of the magnetosphere closely resembles that of a

tilted pulsar, akin to a recently proposed *black hole pulsar* state (Selvi et al. 2024). We present detailed discussions on this transient BH pulsar in later sections.

#### 4.2. Rotation and alignment of current sheets

The spinning remnant BH induces a rotation of the magnetic field lines and the current sheets via frame dragging with respect to its spin axis. In the following, we would like to track the motion of current sheets. These are easily identified with the (toroidal) electric current,  $j^\phi$ , which we here approximate via its Newtonian expression,

$$j^\phi \approx \epsilon^{\phi ij} \partial_i B_j. \quad (2)$$

<sup>4</sup> When computing the horizon angular velocity  $\Omega_H$ , we used the mean radius of the instantaneous apparent horizon of the BH.

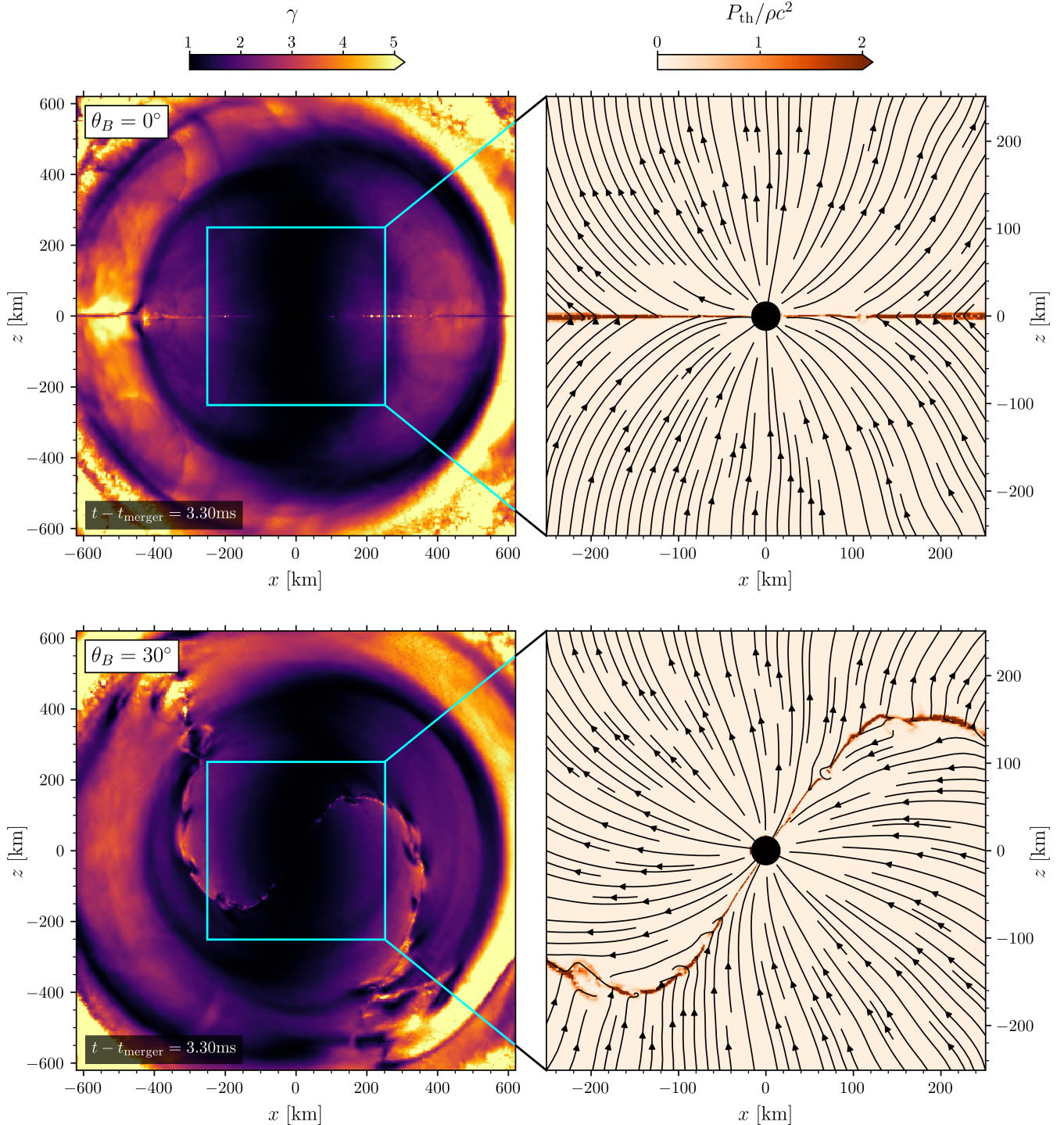


**Figure 4.** Post-merger magnetosphere of the remnant black hole having settled down to a rotating split monopole. The physical quantities are shown in the  $xz$  plane. Left: fluid Lorentz factor  $\gamma$ . Right: ratio of the thermal pressure  $p_{\text{th}}$  to the rest energy density  $\rho c^2$ . Black solid lines show the in-plane magnetic field lines. An equatorial current sheet is formed at which the magnetic field lines in upper and lower hemispheres reconnect, dissipating magnetic energy and causing a flux decay (balding) of the BH. The inner magnetosphere is driven to co-rotate with the BH due to frame dragging. As a result, the post-merger magnetosphere of an inclined model (e.g.  $\theta_B = 30^\circ$ , bottom panels) exhibits features similar to those of tilted pulsars (see also Fig. 10). The spin axis of the BH is along  $\hat{z}$  in all models.

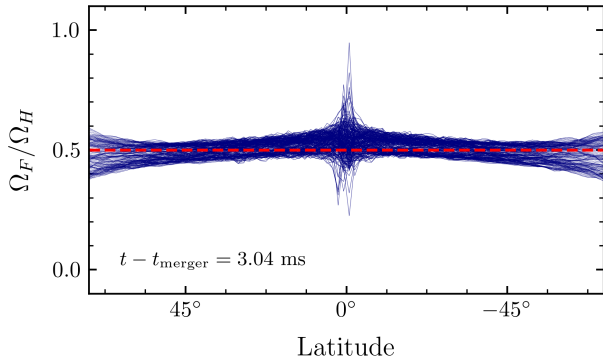


**Figure 5.** Angular velocity of magnetic field lines threading the apparent BH horizon for  $\theta_B = 0^\circ$  simulation. Shown are the distribution of  $\Omega_F$  for each latitude and the stationary axisymmetric force-free solution  $\Omega_F \simeq \Omega_H/2$  (red dashed line).

We then analyze the time evolution of the current on a fixed spherical surface of radius  $r = 2.4r_g$ . In Fig. 6, we show the distribution of  $|j^\phi|$  on the meridional arc  $\phi = 0$  ( $x > 0, y = 0$ ) for all simulations. The equatorial current sheet in the aligned case ( $\theta_B = 0^\circ$ ) does not exhibit notable modulations in its latitude, where we have confirmed in Sec. 4.1 that the magnetosphere is in fact rotating with  $\Omega_F = 0.5\Omega_H$ . For the inclined cases, rotation of the current sheet is clearly seen in Fig. 6. The time interval between neighboring peaks is about 3.5 ms, revealing that the current sheet is rotating with about half of the horizon angular velocity.

Over each meridional lines ( $\phi = \text{const.}$ ) on the spherical surface  $r = 2.4r_g$ , we collect the latitude  $\alpha_0(\phi)$  with the maximum value of  $|j^\phi|$ , which is effectively the latitude of the current sheet at that azimuthal angle. Then we define the current sheet inclination angle  $\chi$  as<sup>5</sup>

$$\chi = \frac{\max[\alpha_0(\phi)] - \min[\alpha_0(\phi)]}{2}. \quad (3)$$

In Fig. 7, we show the measured  $\chi(t)$  from  $\theta_B = 30^\circ, 60^\circ$  simulations. A nonlinear deformation of the NS during the merger is found to greatly enhance the inclination angle of the magnetic field around the merger remnant, resulting in  $\chi \approx 60^\circ$  for  $\theta_B = 30^\circ$ . We observe a gradual decay in  $\chi(t)$  for both models, indicating the alignment of the current sheet with respect to the BH spin axis over time, which is consistent with the result of Selvi et al. (2024). However, here we can only provide a crude estimate on the alignment timescale  $\tau_\chi \approx 1000\text{--}2000 r_g/c$ , being limited by a short simulation time and a mild spin

<sup>5</sup> See the section 3 of Selvi et al. (2024) for an alternative method to measure  $\chi(t)$  in terms of the magnetic moment.

of the BH. We also caution that the observed alignment timescale could be affected by a high numerical dissipation (see Sec. 4.3).

#### 4.3. Balding and ring-down of the remnant BH

In a split-monopole magnetosphere of a stationary BH, the total magnetic flux threading the horizon

$$\Phi_B = \frac{1}{2} \oint |B^r| d\Omega, \quad (4)$$

exponentially decays as a result of magnetic reconnection in the current sheet (Lyutikov & McKinney 2011; Bransgrove et al. 2021; Selvi et al. 2024). In the top panel of Fig. 8, we show the decay of the horizon magnetic flux  $\Phi_B$  for all simulations. Overall, the decay times shown in Fig. 8 are an order of magnitude shorter than those from the MHD simulations of Bransgrove et al. (2021) and Selvi et al. (2024). This is likely due to artificially high numerical resistivity (i.e., low spatial grid resolution) compared to those studies. At higher resolution than we use, our MHD solution will equally not be able to recover the correct collisionless reconnection rate (Sironi & Spitkovsky 2014; Bransgrove et al. 2021). We therefore treat our results mainly qualitatively, in that the BH pulsar forms and balds, and defer quantitative conclusions to an analytical model discussed in Sec. 4.4.

The magnetic flux decay timescale  $\tau_\Phi$  is almost identical for both of the inclined models, while the aligned model exhibits about 30% faster decay until  $t - t_{\text{merger}} \lesssim 6\text{ms}$ . However, in a split monopole magnetosphere of a stationary Kerr BH, the timescale  $\tau_\Phi$  may not notably depend on the current sheet inclination angle  $\chi$  (Selvi et al. 2024). We investigate the origin of the accelerated magnetic flux decay by examining additional physical quantities, as follows.

Electromagnetic and gravitational perturbations around a BH can be analyzed by means of the Newman-Penrose (NP) scalars (Teukolsky 1972, 1973)

$$\psi_4 = -C_{abcd} n^a \bar{m}^b n^c \bar{m}^d, \quad (5)$$

$$\phi_2 = F_{ab} \bar{m}^a n^b, \quad (6)$$

where  $C_{abcd}$  is the Weyl tensor,  $F_{ab}$  is the electromagnetic field tensor, and  $(l^a, n^a, m^a, \bar{m}^a)$  are orthonormal null tetrads

$$l^a = (t^a + r^a)/\sqrt{2}, \quad (7)$$

$$n^a = (t^a - r^a)/\sqrt{2}, \quad (8)$$

$$m^a = (\theta^a + i\phi^a)/\sqrt{2}. \quad (9)$$

We use the dominant  $(l, m) = (2, 2)$  quadrupole mode of  $\psi_4$  to monitor the BH ringdown, and the  $(l, m) = (1, 1)$



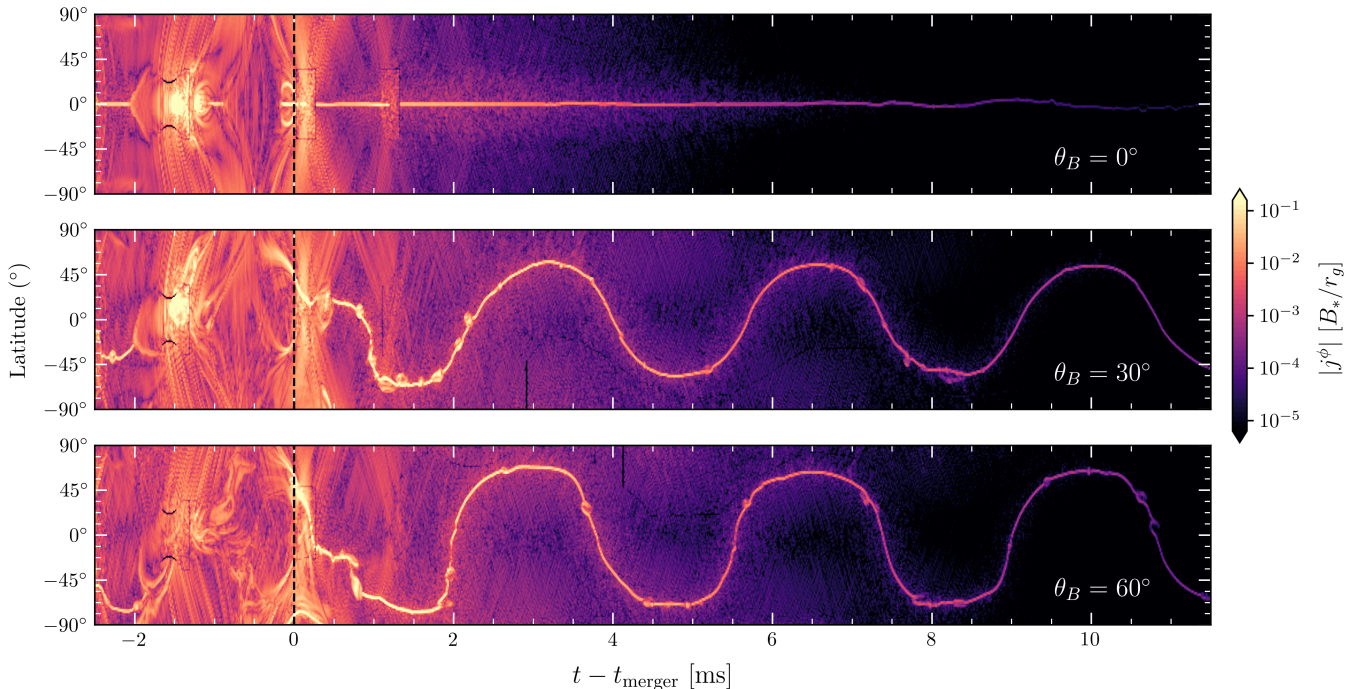


**Figure 6.** A spacetime diagram of the approximate electric current  $|j^\phi|$  on a meridional arc  $\phi = 0$  at  $r = 2.4r_g$  in three simulations with different initial inclinations of the NS magnetic dipole moment ( $\theta_B = 0^\circ, 30^\circ, 60^\circ$ ), displaying the latitude of the post-merger magnetospheric BH current sheet. For the inclined models ( $\theta_B = 30^\circ, 60^\circ$ ), the periodic oscillation in the latitude represents the rotation of the inclined current sheet. The orbital current sheet of the NS in the inspiral phase is also visible for  $t - t_{\text{merger}} \lesssim -2$  ms, where  $t_{\text{merger}}$  indicates the merger time.

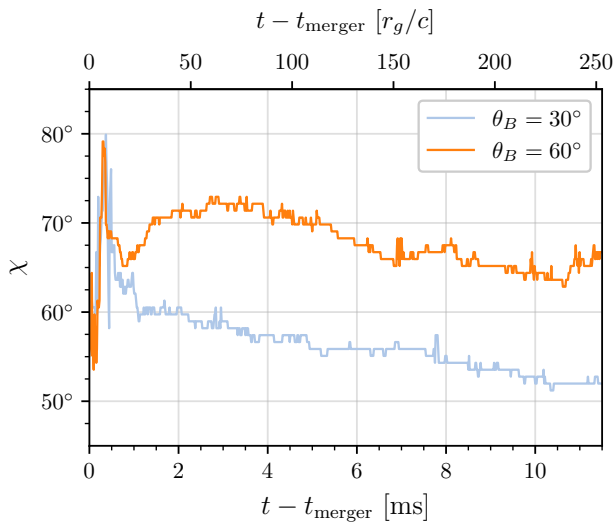


**Figure 7.** Time evolution of the current sheet inclination angle  $\chi$  for the  $\theta_B = 30^\circ, 60^\circ$  models.

dipole mode of  $\phi_2$  to monitor the electromagnetic mod-

ulation in the magnetosphere.<sup>6</sup> We show the imaginary part of  $\phi_2^{(l=1, m=1)}$  and  $\psi_4^{(l=2, m=2)}$  (hereafter denoted simply as  $\phi_2$  and  $\psi_4$  for brevity) in the middle and lower panels of Fig. 8. In the following discussions, we denote the exponential decay time scale of the NP scalar  $\phi_2$  ( $\psi_4$ ) as  $\tau_\phi^{\text{NP}}$  ( $\tau_\psi^{\text{NP}}$ ).

We compute the quasi-normal mode (QNM) frequencies of the remnant BH for  $(s, l, m) = (-2, 2, 2)$  and  $(s, l, m) = (-1, 1, 1)$  fundamental modes using the `qnm` package (Stein 2019). The imaginary parts of the two QNM frequencies are both around  $12r_g/c$ . From the real parts, we obtain the oscillation period 0.94ms for  $\phi_2$  and 0.59ms for  $\psi_4$ . The damped sinusoidal oscilla-

<sup>6</sup> The NP scalar  $\psi_4$  corresponds to the outgoing gravitational radiation at null infinity. The Maxwell NP scalar  $\phi_2$  is proportional to the complex electric field  $E_\theta + iE_\phi$ . In an axisymmetric background magnetic field,  $E_\theta$  corresponds to the Alfvénic modes and  $E_\phi$  to the fast magnetosonic modes.

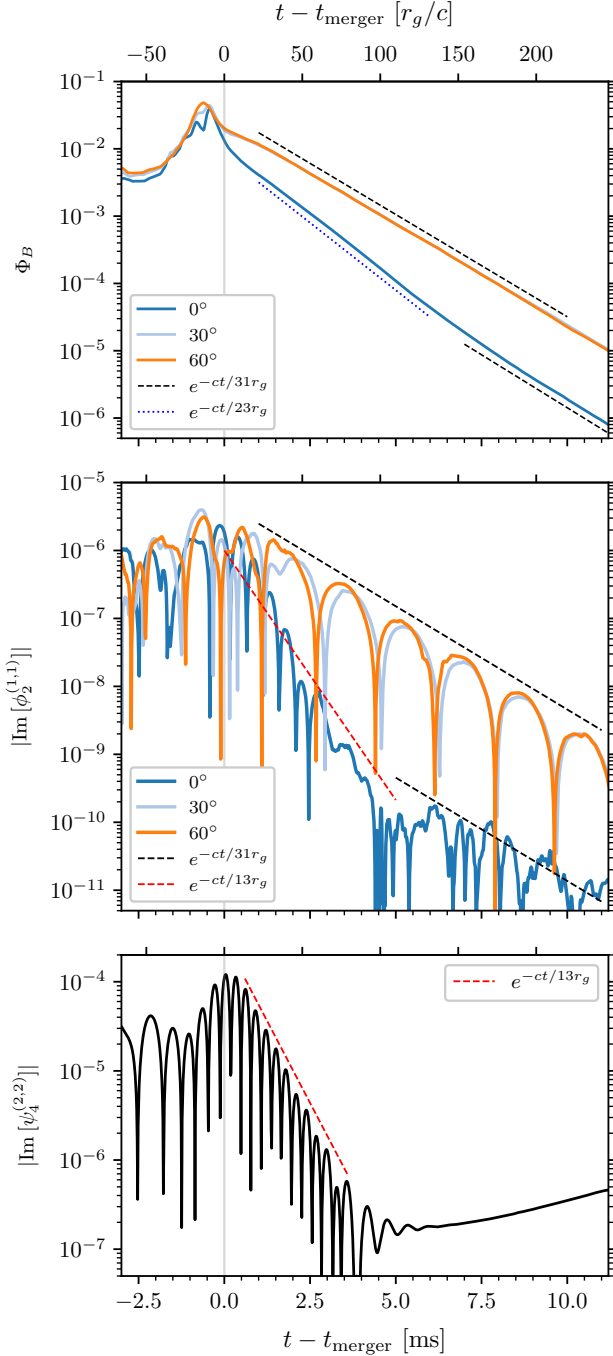


**Figure 8.** Top: total magnetic flux extracted on a spherical surface  $r = 2.4r_g$  near the apparent horizon. The result from  $\theta_B = 30^\circ$  (cyan solid line) and  $\theta_B = 60^\circ$  (orange solid line) are lying almost on top of each other. Middle: imaginary part of  $(l, m) = (1, 1)$  mode of the Maxwell Newman-Penrose (NP) scalar  $\phi_2$  extracted at  $r = 4.3r_g$ . Bottom: imaginary part of  $(l, m) = (2, 2)$  mode of the NP scalar  $\psi_4$  extracted at  $r = 4.3r_g$ . We only show the result from  $\theta_B = 0^\circ$  since the result is almost identical for all simulations. Exponential decays with timescales  $31r_g/c$ ,  $23r_g/c$  and  $13r_g/c$  are indicated by the black dashed, blue dotted, and red dashed lines.

tion of  $\psi_4$ , shown in the bottom panel of Fig. 8, agrees well with both real and imaginary parts of the computed QNM frequency.

*Inclined magnetic field* ( $\theta_B = 30^\circ, 60^\circ$ ) — Both simulations show  $\tau_\phi^{\text{NP}} = 31r_g/c$ , which is the same as their magnetic flux decaying timescale  $\tau_\Phi$ . Periodic oscillations of  $\phi_2$  for  $t - t_{\text{merger}} \gtrsim 1.5\text{ms}$  are coming from the rotation of current sheets (see Fig. 6), which has a half-period of  $2\pi/\Omega_H \approx 1.8\text{ms}$ . From the fact that the measured decay timescales  $\tau_\Phi$  and  $\tau_\phi^{\text{NP}}$  not only agree with each other but also being disparate from the QNM frequency, we deduce that  $\tau_\Phi = 31r_g/c$  is the the flux decay timescale of the BH pulsar due to magnetic reconnection in our setup, and the time decay of  $\phi_2$  is simply a consequence of the declining magnetic field strength.

*Aligned magnetic field* ( $\theta_B = 0^\circ$ ) — In the early phase of the ringdown ( $t - t_{\text{merger}} \leq 5\text{ms}$ ),  $\phi_2$  exhibits a rapid decay with  $\tau_\phi^{\text{NP}} \approx \tau_\psi^{\text{NP}}$ . The period of the oscillations in  $\phi_2$ , which lasts about 2.5 cycles, is measured to be 0.9ms and shows a good agreement with the QNM frequency (0.94ms). This indicates that the evolution of the post-merger magnetosphere is dominated by the ringdown of the BH, which rapidly sheds off magnetic fluxes from the horizon. We show  $\phi_2$  in the meridional ( $xz$ ) plane in Fig. 9. The magnetic flux shedding driven by QNMs induces episodes of quasi-periodic modulations in the magnetosphere, which leads to a more rapid reconnection of the field lines on the equatorial plane. The same process has been also observed by Most et al. (2024a) for the gravitational collapse of a NS with its spin axis aligned with the magnetic moment. On the other hand, both  $\tau_\Phi$  and  $\tau_\phi^{\text{NP}}$  are slowed down to  $\approx 31r_g/c$  later in  $t - t_{\text{merger}} \geq 6\text{ms}$ , implying that the balding process of the BH begins to be affected more by resistivity. The magnetic flux shedding by QNMs becomes subdominant as gravitational perturbations fade out, then the flux decay is governed by magnetic reconnection afterwards. We caution that this observed behavior may change at higher numerical resolutions, which will exhibit a better scale separation between plasma and gravitational effects.

#### 4.4. Striped wind

The rotation of an inclined split-monopole magnetosphere on a BH leads to a striped wind (Selvi et al. 2024) which appears to be similar to those from oblique pulsars (e.g. Michel 1982; Petri 2012; Tchekhovskoy et al. 2013; Cerutti & Philippov 2017), albeit without the presence of a closed zone. We illustrate this in Fig. 10 for the  $\theta_B = 30^\circ$  simulation, where the sign change in the toroidal magnetic field is clearly visible. Different from a stationary pulsar solution with  $B^\phi \sim 1/r$  (Michel

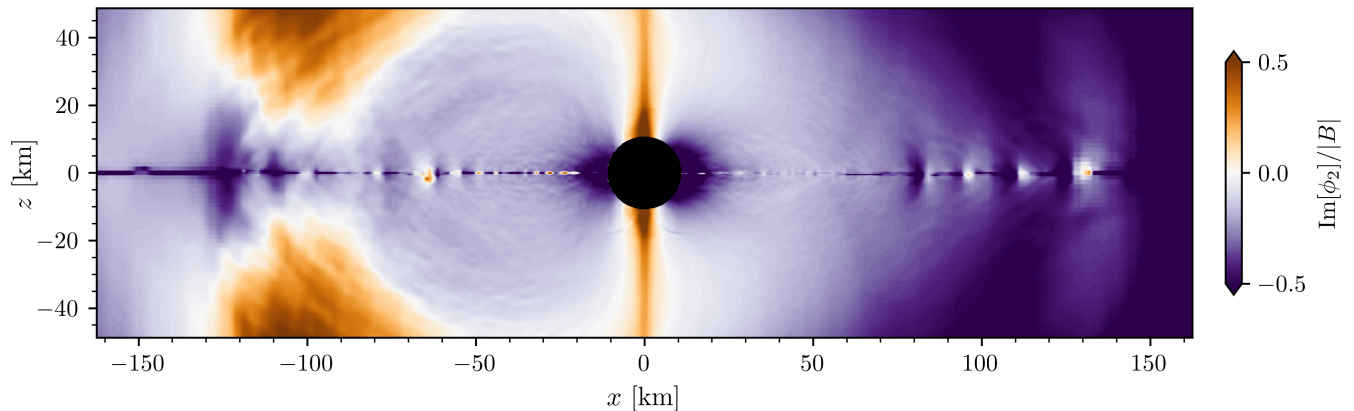


**Figure 9.** Imaginary part of the Maxwell Newman-Penrose scalar  $\phi_2^{(l=1,m=1)}$ , corresponding approximately to outgoing fast magnetosonic waves, on the vertical ( $xz$ ) plane normalized with the magnitude of magnetic field for the aligned case  $\theta_B = 0^\circ$  at  $t - t_{\text{merger}} = 1.05$  ms.

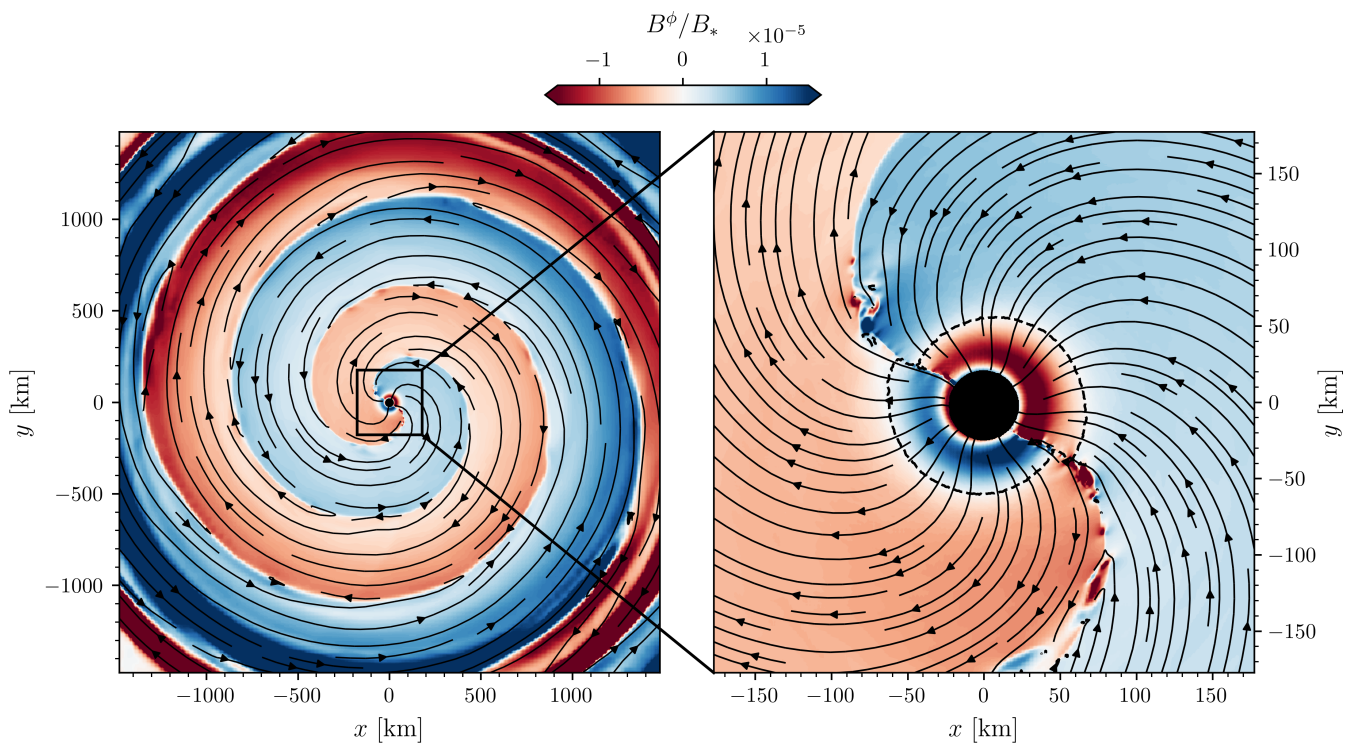


**Figure 10.** Pulsar-like striped wind from the remnant black hole at  $t - t_{\text{merger}} = 7.0$ ms from  $\theta_B = 30^\circ$  simulation. We show the toroidal magnetic field  $B^\phi$  with the magnetic field lines on the equatorial ( $xy$ ) plane in both panels. The remnant black hole is shown with a black circle and spinning counter clockwise in this figure. In the right panel, we show the stagnation surface ( $u^r = 0$ ) with a black dashed line.

1982; Bogovalov 1999), the magnetic field here decays over time. While this will not affect the geometry of the striped wind, its amplitude will naturally become a function of retarded time,  $B^\phi = B^\phi(r, \theta, t - r/c)$ , as can be seen from the left panel of Fig. 10.

A stagnation surface at which  $u^r = 0$ , separating the inflow and outflow region of the plasma, appears in the

vicinity of the BH (Bransgrove et al. 2021); we show it on the right panel of Fig. 10. Interestingly, the stagnation surface is discontinuous across the rotating current sheet, with its radius being greater at the upstream of the current sheet (trailing part of the striped wind), appearing as a half-split spheroid with an offset along the current sheet.

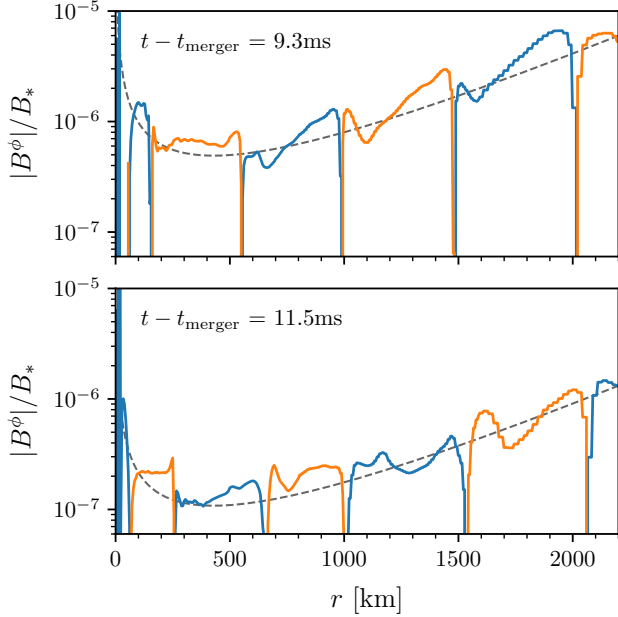


**Figure 11.** Toroidal magnetic field of the striped wind  $|B^\phi(r)|$  on the equatorial plane along the  $\hat{x}$  axis. Alternating signs (polarities) of  $B^\phi$  in each stripes are denoted with different colors. The dashed line shows the fit with Eq. (11).

We also find that the rotation angular velocity of the magnetic field lines is slower (faster) at the upstream (downstream) of the rotating current sheet, exhibiting a symmetric deviation from  $\Omega_F = \Omega_H/2$ . We reserve a more detailed analysis of these near-horizon dynamics of oblique BH pulsars for future work.

An analytic model of the toroidal magnetic field  $B^\phi$  in the wind can be developed as follows. For a nearly force-free wind from a rotating split-monopole,  $B^\phi$  can be approximated as (Michel 1982; Bogovalov 1999; Tchekhovskoy et al. 2016)

$$|B^\phi(r, \theta)| \approx \frac{\Omega r \sin \theta}{c} |B_r| = \frac{\Omega B_* r_*^2 \sin \theta}{c r}, \quad (10)$$

where  $\Omega$  is the rotation angular velocity,  $B_*$  is the surface magnetic field strength, and  $r_*$  is the radius of the rotator. For a BH pulsar, we can replace the angular velocity  $\Omega$  with  $\Omega_F = \Omega_H/2$ , the radius  $r_*$  with  $r_H$ , and the surface magnetic field  $B_*$  with  $B_H(t) = B_{H,0} e^{-t/\tau_\Phi}$ . The resulting extension of Eq. (10) for a BH pulsar is

$$|B^\phi(r, \theta, t)| = \frac{\Omega_H B_{H,0} r_H^2 e^{-(t-r/c)/\tau_\Phi} \sin \theta}{2c r}, \quad (11)$$

where  $(t - r/c)$  accounts for a retarded time.

Fig. 11 compares the  $\theta_B = 30^\circ$  simulation data with Eq. (11) on the equatorial plane, using  $\tau_\Phi = 31r_g/c$  measured from the balding process (Sec. 4.3) and shifting  $t \rightarrow t - t_{\text{merger}}$ . Our approximate analytic model shows a

good agreement with the simulation result. The value of  $B_{H,0}$  fitted from the simulation data is  $1.5 \times 10^{-2} B_*$ , revealing that the split-monopole BH pulsar inherits about 1% of the magnetic field strength from the companion NS. A separate estimate from the BH magnetic flux  $\Phi_B = 2\pi r_H^2 B_{H,0}$  (top panel of Fig. 8) yields almost the same value of  $B_{H,0}$ , reassuring the validity of the analytic model Eq. (11) as well as the measured value of  $B_{H,0}$ .

#### 4.5. Energetics

The wind from the BH pulsar is powered by the energy extracted from the remnant BH through the Blandford-Znajek (BZ) process (Blandford & Znajek 1977), leading to a spin-down of the BH. The spin-down power of an aligned split-monopole magnetosphere, to a leading order of the BH spin,<sup>7</sup> is given as (Tchekhovskoy et al. 2010)

$$P_{\text{BZ}} = \frac{(\Phi_B^2/4\pi)\Omega_H^2}{6\pi c}. \quad (12)$$

The BZ power (12) can be written into a form more commonly used in the pulsar literature

$$L = \frac{2}{3c} \Omega_F^2 B_H^2 r_H^4, \quad (13)$$

with  $\Omega_F = \Omega_H/2$  and  $\Phi_B = 2\pi r_H^2 B_H$ .

The spin-down power (Eq. (12) or (13)) is carried by the electromagnetic Poynting flux, which is not a direct observable. It is the dissipation in the current sheets which converts the electromagnetic field energy of the wind into kinetic energy of particles and subsequent electromagnetic emissions (e.g. Philippov et al. 2019). In a steady pulsar magnetosphere, about 10–20 percent of the spin-down power can be dissipated within 10 light cylinder radii (e.g., Parfrey et al. 2012; Chen & Beloborodov 2014; Philippov et al. 2015, see also Cerutti & Beloborodov (2017) for a review).

Here we develop a toy model for the dissipation luminosity of a BH pulsar, closely following the approach by Cerutti et al. (2020). From here we will use  $t$  to denote the time after the formation of the split monopole i.e.  $(t - t_{\text{merger}}) \rightarrow t$ . The total dissipation luminosity is given by a volume integral

$$\begin{aligned} L_D &= \int (\mathbf{J} \cdot \mathbf{E}) r^2 \sin \theta dr d\theta d\phi \\ &= \frac{c\beta_{\text{rec}}}{\pi} \int (B^\phi)^2 r \sin \theta dr d\theta, \end{aligned} \quad (14)$$

<sup>7</sup> The relative correction from the next order term  $\propto (\Omega_H)^4$  is less than  $10^{-3}$  in our case. See Tchekhovskoy et al. (2010) for the expansion formula up to  $(\Omega_H)^6$ .

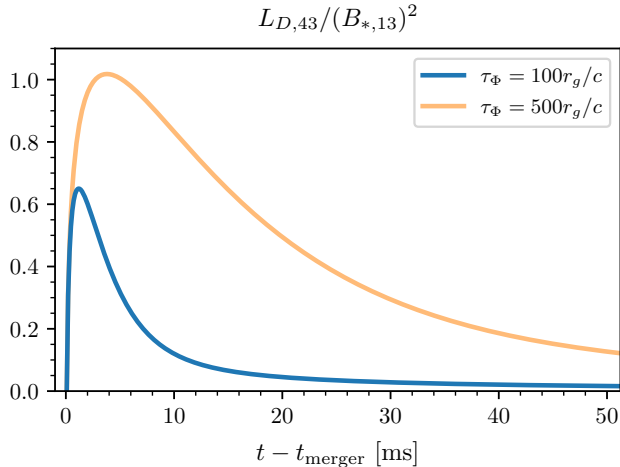


**Figure 12.** The dissipation luminosity from a BH pulsar  $L_D(t)$  computed with an analytic model developed in Sec. 4.5, normalized with  $L_{D,43} \equiv L_D/(10^{43} \text{erg s}^{-1})$  and  $B_{*,13} \equiv B_*/(10^{13} \text{G})$ . Due to a high (unphysical) numerical resistivity in our simulation, we construct the light curves using  $\tau_\Phi = 100r_g/c$  (blue solid line) and  $\tau_\Phi = 500r_g/c$  (orange solid line) consistent with bounds from high-resolution kinetic simulations of Bransgrove et al. (2021).

where  $\beta_{\text{rec}}$  is the dimensionless reconnection rate (Uzdensky & Spitkovsky 2014). A primary difference of our toy model from that of Cerutti et al. (2020) is the exponential damping term in the Eq. (11) associated with the flux decay of the BH. Substituting the expression (11) into (14) and performing angular integration,

$$L_D = \frac{2\beta_{\text{rec}}L_0}{\pi} e^{-2t/\tau_\Phi} \int_{r_{\text{min}}}^{r_{\text{max}}} \frac{e^{2r/c\tau_\Phi}}{r} dr, \quad (15)$$

where  $L_0 = (2/3c)\Omega_F^2 B_{H,0}^2 r_H^4$  is an instantaneous BZ power of the BH pulsar at  $t = 0$ . The upper and lower bounds of the integral in Eq. (15) correspond to the radial extent of the striped wind,  $r_{\text{min}} = r_H$  and  $r_{\text{max}} \approx ct$ , which gives

$$L_D(t) = \frac{2\beta_{\text{rec}}L_0}{\pi} e^{-2t/\tau_\Phi} \left[ \text{Ei} \left( \frac{2t}{\tau_\Phi} \right) - \text{Ei} \left( \frac{2r_H}{c\tau_\Phi} \right) \right], \quad (16)$$

where  $\text{Ei}(x) = \int_{-\infty}^x (e^t/t) dt$  is the exponential integral.

We apply our toy model to the  $\theta_B = 30^\circ$  simulation. The initial spin-down power  $L_0$  can be computed from the mass and spin of the remnant BH, and using  $B_{H,0}/B_* = 1.5\%$  fitted from the simulation result (see Sec. 4.4).<sup>8</sup> The flux decay timescale  $\tau_\Phi = 31r_g/c$

<sup>8</sup> Note that this ratio  $B_{H,0}/B_*$ , namely the portion of the magnetic flux that a nascent BH pulsar inherits from the swallowed NS, can only be probed with a full numerical relativity merger simulation as performed here.

from our simulation is dominated by unphysical numerical resistivity, therefore we consider  $\tau_\Phi = 100r_g/c$  and  $\tau_\Phi = 500r_g/c$  motivated from the high-resolution (kinetic) simulations of Bransgrove et al. (2021) as a more realistic input for assessing light curves. The reconnection rate is fixed to  $\beta_{\text{rec}} = 0.1$  from kinetic plasma simulations (Sironi & Spitkovsky 2014).

In Fig. 12, we show the modelled dissipation luminosity  $L_D(t)$  scaled with the initial NS magnetic field strength. The time curve of the dissipation luminosity exhibits a rapid rise to its peak value within a few milliseconds, followed by exponential then power-law decay over tens of milliseconds. A magnetar can power a burst with the luminosity  $\sim 10^{47} \text{erg s}^{-1}$ , while a NS with  $B_* \sim 10^{12} \text{G}$  will emit a relatively faint one with  $\sim 10^{41} \text{erg s}^{-1}$ . The exponential factor  $e^{2r/c\tau_\Phi}$  in Eq. (15) suggests that the region  $r \approx r_{\text{max}}$  is predominantly contributing to the total integral, implying the forefront of the expanding striped wind with a thickness  $\Delta r \approx c\tau_\Phi$  is mainly powering the total dissipation luminosity.

The total dissipated energy  $E = \int L_D(t) dt$  does not converge due to a  $t^{-1}$  asymptotic decay of  $L_D(t)$ . Realistically, dissipation in the current sheets would introduce a faster decrease of  $B^\phi$  in radius, and the decay of  $B_H(t)$  below a certain threshold can halt the pair production around the BH, turning off the BH pulsar. Naively setting the end time of the burst as when  $L_D(t)$  drops down to 1/10 of its peak value, the burst lasts about 15 ms (60 ms) for  $\tau_\Phi = 100r_g/c$  ( $500r_g/c$ ), with the average luminosity  $2.6 \times 10^{43} \text{erg s}^{-1}$  ( $4.2 \times 10^{43} \text{erg s}^{-1}$ ) for  $B_* = 10^{13} \text{G}$ .

## 5. ELECTROMAGNETIC TRANSIENT

### 5.1. Radio burst

The power dissipated in monster shocks at small radii is immediately radiated in X-rays (Beloborodov 2023). Later, when the shock expands to larger radii, it can become a bright source of radio emission and emit a powerful fast radio burst (FRB). Magnetized shocks emit a radio precursor by the synchrotron maser mechanism; it was initially proposed for termination shocks of pulsar winds (Hoshino et al. 1992; Lyubarsky 2014) and then for internal shocks in magnetized  $e^\pm$  outflows to explain repeating FRBs (Beloborodov 2017).

Consider first the monster shock at small radii  $r \sim 10^7\text{--}10^8 \text{cm}$ . Kinetic plasma simulations of magnetized shocks (Sironi et al. 2021; Vanthieghem & Levinson 2025) show precursor emission with frequency  $\omega_{\text{pre}} \sim 3\tilde{\omega}_B = 3e\tilde{B}/m_e c$ , where  $\tilde{B}$  is the upstream magnetic field measured in the plasma rest frame,  $e$  is the elementary charge, and  $m_e$  is the electron mass.  $\tilde{B}$  is reduced

from the background value  $B_{\text{bg}}$  by the strong expansion of the plasma ahead of the monster shock (Beloborodov 2023):

$$\tilde{B} \approx \frac{\omega r}{2c\sigma_{\text{bg}}} B_{\text{bg}}, \quad (17)$$

where  $\sigma_{\text{bg}} = B_{\text{bg}}^2 / 4\pi n_{\text{bg}} m_e c^2$  is the background magnetization parameter, and  $\omega$  is the frequency of the magnetospheric perturbation that led to shock formation (our simulation shows  $\omega r/c \sim 10$ ). Density  $n_{\text{bg}}$  can be parameterized by multiplicity  $\mathcal{M} \equiv n_{\text{bg}}/n_0$ , where  $n_0 = \nabla \cdot \mathbf{E} / 4\pi e \sim \Omega B_{\text{bg}} / 2\pi e c$  is the minimum density required to support the magnetospheric rotation with drift speed  $\sim \Omega r$  (Goldreich & Julian 1969). This gives  $\omega_{\text{pre}} \sim (r\omega/c)\mathcal{M}\Omega \sim 10^4 \mathcal{M}$  rad/s. This simple estimate is, however, deficient because it neglects the deceleration of the upstream flow by strong radiative losses. Losses dramatically change the radio precursor from monster shocks at small radii by increasing its frequency and suppressing its power (Beloborodov, in preparation).

Powerful radio emission is expected from the relativistic shock when it expands far into the  $e^\pm$  outflow, reaching  $r \sim 10^{13}\text{--}10^{14}$  cm (Beloborodov 2017, 2020). Then, a fraction  $\sim 10^{-4}$  of the blast wave power is expected to convert to radio waves, whose frequency decreases with time (proportionally to the local  $B$ ) and passes through the GHz band, best for radio observations. In this paper, we do not follow the outflow dynamics with shocks at large radii; however, this may become possible for future MHD simulations. Our simulation shows that shocks launched from NS-BH mergers are asymmetric, but not strongly collimated. Therefore, they can produce FRBs observable for a broad range of line of sights. Note that no baryonic ejecta are expected from BH swallowing a NS, so nothing should block the FRB from observers.

### 5.2. Gamma-ray burst

The X-ray transient expected from the simulated merger is powered by dissipation of magnetospheric energy. Two dissipation mechanisms are observed in the simulation: shocks and magnetic reconnection in the split-monopole current sheet around the BH after the merger. Dissipation occurs at small radii, which correspond to a large compactness parameter  $\ell = \sigma_{\text{T}} L / r m_e c^3$ , where  $L$  is the dissipation power and  $\sigma_{\text{T}}$  is the Thompson cross section. Note that  $L$  and  $\ell$  scale as  $B^2$ . For a strongly magnetized NS, e.g. with  $B \sim 10^{14}$  G, the huge  $\ell$  implies that the dissipated energy becomes immediately thermalized. Thus, the merger ejects a hot “fireball” – a thermalized, magnetically dominated  $e^\pm$  outflow. As the outflow expands to larger radii, it adiabatically cools,  $e^\pm$  annihilate and release a burst of quasi-thermal radiation similar to the

GRB from the magnetar collapse described in Most et al. (2024a).

An additional dissipation mechanism is expected to operate in the outflow at large radii, and can add a nonthermal tail to the GRB spectrum. It is caused by the striped structure of the outflow, similar to the striped winds from pulsars. The stripes develop current sheets where magnetic reconnection gradually dissipates the alternating magnetic flux (Lyubarsky & Kirk 2001; Cerutti et al. 2020). A similar mechanism was previously proposed to operate in canonical GRBs (Drenkhahn & Spruit 2002). It will release energy after the outflow becomes optically thin (which happens quickly in the baryon-free outflow from BH–NS merger). Therefore, it can generate energetic particles, emitting a nonthermal component of the GRB.

## 6. CONCLUSIONS

We have presented a detailed numerical investigation into the magnetospheric dynamics of BH–NS mergers without tidal disruption. Using GRMHD simulations capable of probing the near force-free limit, we identify two mechanisms for generating an electromagnetic transient.

First, we observe that fast magnetosonic waves are launched into the magnetosphere of the NS before it plunges into the BH. These waves, as expanding outward with almost the speed of light, develop into monster shocks due to a more rapidly decaying ambient magnetic field (Beloborodov 2023). The full MHD simulation is essential for tracking this effect, so it could not be captured by earlier vacuum or force-free simulations. The launched shocks are expected to emit a bright radio transient when they expand to large radii.

When the BH swallows the NS together with its magnetic dipole moment, its external magnetosphere quickly rearranges itself into a split-monopole configuration with a large-scale current sheet. Then, the BH gradually loses the acquired “magnetic hair.” This balding is assisted by magnetic reconnection and gravitational effects (QNMs). The relative importance of these two processes varies over time and depends on the misalignment between the magnetic dipole moment and the BH spin. The split monopole is dragged into rotation by the BH and forms a transient BH pulsar which can power a post-merger EM signal in the X-ray and  $\gamma$ -ray band.

The monster shocks and the balding BH pulsar were previously studied in symmetric setups with a single compact object (Bransgrove et al. 2021; Beloborodov 2023; Most et al. 2024a; Selvi et al. 2024). Our ab-initio simulations demonstrate how both phenomena naturally

occur in the complex dynamical spacetime of the BH–NS merger.

The binary parameters considered in our work are representative of the BH–NS mergers detected to date (Abac et al. 2024), implying that shock formation from magnetosonic waves and the emergence of a BH pulsar could be a common outcome for the BH–NS populations observable with ground-based GW detectors such as the LIGO/Virgo/KAGRA network.

#### ACKNOWLEDGMENTS

The authors are grateful to Ashley Bransgrove, Koushik Chatterjee, Alexander Chernoglazov, Amir Levinson, Keefe Mitman, Alexander Philippov, Eliot Quataert, Sebastiaan Selvi, Lorenzo Sironi, Anatoly Spitkovsky, Alexander Tchekhovskoy, Saul Teukolsky, Christopher Thompson, and Yici Zhong for insightful comments and discussions. YK acknowledges support by the Sherman Fairchild Foundation and by NSF Grants No. PHY-2309211, No. PHY-2309231, and No. OAC-2209656 at Caltech. ERM acknowledges support by the National Science Foundation under grants No. PHY-2309210 and AST-2307394, and from NASA’s ATP program under grant 80NSSC24K1229. AMB acknowledges support by NASA grants 80NSSC24K1229 and 21-ATP21-0056,

and Simons Foundation grant No. 446228. BR acknowledges support by the Natural Sciences & Engineering Research Council of Canada (NSERC), the Canadian Space Agency (23JWGO2A01), and by a grant from the Simons Foundation (MP-SCMPS-00001470). BR acknowledges a guest researcher position at the Flatiron Institute, supported by the Simons Foundation.

Simulations were performed on the NSF Frontera supercomputer at the Texas Advanced Computing Center under grant AST21006, and on the Delta cluster at the National Center for Supercomputing Applications (NCSA) through allocation PHY210074 from the Advanced Cyberinfrastructure Coordination Ecosystem: Services & Support (ACCESS) program, which is supported by National Science Foundation grants #2138259, #2138286, #2138307, #2137603, and #2138296.

*Software:* EinsteinToolkit (Loffler et al. 2012), Frankfurt/IllinoisGRMHD (Most et al. 2019; Etienne et al. 2015) FUKA (Papenfort et al. 2021), Kadath (Grandclement 2010), AHFinderDirect (Thornburg 2004), kuibit (Bozzola 2021), matplotlib (The Matplotlib Development Team 2024), numpy (Harris et al. 2020), scipy (Gommers et al. 2024), qnm (Stein 2019)

#### REFERENCES

- Abac, A. G., et al. 2024, *Astrophys. J. Lett.*, 970, L34, doi: [10.3847/2041-8213/ad5beb](https://doi.org/10.3847/2041-8213/ad5beb)
- Abbott, R., et al. 2020, *Astrophys. J. Lett.*, 896, L44, doi: [10.3847/2041-8213/ab960f](https://doi.org/10.3847/2041-8213/ab960f)
- . 2021, *Astrophys. J. Lett.*, 915, L5, doi: [10.3847/2041-8213/ac082e](https://doi.org/10.3847/2041-8213/ac082e)
- Akmal, A., Pandharipande, V. R., & Ravenhall, D. G. 1998, *Phys. Rev. C*, 58, 1804, doi: [10.1103/PhysRevC.58.1804](https://doi.org/10.1103/PhysRevC.58.1804)
- Alcubierre, M., Bruegmann, B., Diener, P., et al. 2003, *Phys. Rev. D*, 67, 084023, doi: [10.1103/PhysRevD.67.084023](https://doi.org/10.1103/PhysRevD.67.084023)
- Anand, S., et al. 2021, *Nature Astron.*, 5, 46, doi: [10.1038/s41550-020-1183-3](https://doi.org/10.1038/s41550-020-1183-3)
- Armas, J., Cai, Y., Compère, G., Garfinkle, D., & Gralla, S. E. 2020, *JCAP*, 04, 009, doi: [10.1088/1475-7516/2020/04/009](https://doi.org/10.1088/1475-7516/2020/04/009)
- Baumgarte, T. W., & Shapiro, S. L. 2003, *Astrophys. J.*, 585, 930, doi: [10.1086/346104](https://doi.org/10.1086/346104)
- Beloborodov, A. M. 2017, *Astrophys. J. Lett.*, 843, L26, doi: [10.3847/2041-8213/aa78f3](https://doi.org/10.3847/2041-8213/aa78f3)
- . 2020, *Astrophys. J.*, 896, 142, doi: [10.3847/1538-4357/ab83eb](https://doi.org/10.3847/1538-4357/ab83eb)
- . 2021, *Astrophys. J.*, 921, 92, doi: [10.3847/1538-4357/ac17e7](https://doi.org/10.3847/1538-4357/ac17e7)
- . 2023, *Astrophys. J.*, 959, 34, doi: [10.3847/1538-4357/acf659](https://doi.org/10.3847/1538-4357/acf659)
- Bernuzzi, S., & Hilditch, D. 2010, *Phys. Rev. D*, 81, 084003, doi: [10.1103/PhysRevD.81.084003](https://doi.org/10.1103/PhysRevD.81.084003)
- Biscoveanu, S., Landry, P., & Vitale, S. 2022, *Mon. Not. Roy. Astron. Soc.*, 518, 5298, doi: [10.1093/mnras/stac3052](https://doi.org/10.1093/mnras/stac3052)
- Blandford, R. D., & Znajek, R. L. 1977, *Mon. Not. Roy. Astron. Soc.*, 179, 433, doi: [10.1093/mnras/179.3.433](https://doi.org/10.1093/mnras/179.3.433)
- Bogovalov, S. V. 1999, *Astron. Astrophys.*, 349, 1017, doi: [10.48550/arXiv.astro-ph/9907051](https://doi.org/10.48550/arXiv.astro-ph/9907051)
- Bozzola, G. 2021, *The Journal of Open Source Software*, 6, 3099, doi: [10.21105/joss.03099](https://doi.org/10.21105/joss.03099)
- Bransgrove, A., Ripperda, B., & Philippov, A. 2021, *Phys. Rev. Lett.*, 127, 055101, doi: [10.1103/PhysRevLett.127.055101](https://doi.org/10.1103/PhysRevLett.127.055101)
- Carrasco, F., Shibata, M., & Reula, O. 2021, *Phys. Rev. D*, 104, 063004, doi: [10.1103/PhysRevD.104.063004](https://doi.org/10.1103/PhysRevD.104.063004)

- Carrasco, F., Viganò, D., Palenzuela, C., & Pons, J. A. 2019, *Mon. Not. Roy. Astron. Soc.*, 484, L124, doi: [10.1093/mnrasl/slz016](https://doi.org/10.1093/mnrasl/slz016)
- Cerutti, B., & Beloborodov, A. 2017, *Space Sci. Rev.*, 207, 111, doi: [10.1007/s11214-016-0315-7](https://doi.org/10.1007/s11214-016-0315-7)
- Cerutti, B., & Philippov, A. 2017, *Astron. Astrophys.*, 607, A134, doi: [10.1051/0004-6361/201731680](https://doi.org/10.1051/0004-6361/201731680)
- Cerutti, B., Philippov, A. A., & Dubus, G. 2020, *Astron. Astrophys.*, 642, A204, doi: [10.1051/0004-6361/202038618](https://doi.org/10.1051/0004-6361/202038618)
- Chawla, S., Anderson, M., Besselman, M., et al. 2010, *Phys. Rev. Lett.*, 105, 111101, doi: [10.1103/PhysRevLett.105.111101](https://doi.org/10.1103/PhysRevLett.105.111101)
- Chen, A. Y., & Beloborodov, A. M. 2014, *Astrophys. J. Lett.*, 795, L22, doi: [10.1088/2041-8205/795/1/L22](https://doi.org/10.1088/2041-8205/795/1/L22)
- Chen, A. Y., Yuan, Y., Li, X., & Malmann, J. F. 2022, <https://arxiv.org/abs/2210.13506>
- Contopoulos, I., Kazanas, D., & Papadopoulos, D. B. 2013, *Astrophys. J.*, 765, 113, doi: [10.1088/0004-637X/765/2/113](https://doi.org/10.1088/0004-637X/765/2/113)
- Dai, Z. G. 2019, *Astrophys. J. Lett.*, 873, L13, doi: [10.3847/2041-8213/ab0b45](https://doi.org/10.3847/2041-8213/ab0b45)
- Del Zanna, L., Zanotti, O., Bucciantini, N., & Londrillo, P. 2007, *Astron. Astrophys.*, 473, 11, doi: [10.1051/0004-6361:20077093](https://doi.org/10.1051/0004-6361:20077093)
- D’Orazio, D. J., & Levin, J. 2013, *Phys. Rev. D*, 88, 064059, doi: [10.1103/PhysRevD.88.064059](https://doi.org/10.1103/PhysRevD.88.064059)
- D’Orazio, D. J., Levin, J., Murray, N. W., & Price, L. 2016, *Phys. Rev. D*, 94, 023001, doi: [10.1103/PhysRevD.94.023001](https://doi.org/10.1103/PhysRevD.94.023001)
- Drenkhahn, G., & Spruit, H. C. 2002, *Astron. Astrophys.*, 391, 1141, doi: [10.1051/0004-6361:20020839](https://doi.org/10.1051/0004-6361:20020839)
- Duez, M. D., Liu, Y. T., Shapiro, S. L., & Stephens, B. C. 2005, *Phys. Rev. D*, 72, 024028, doi: [10.1103/PhysRevD.72.024028](https://doi.org/10.1103/PhysRevD.72.024028)
- East, W. E., Lehner, L., Liebling, S. L., & Palenzuela, C. 2021, *Astrophys. J. Lett.*, 912, L18, doi: [10.3847/2041-8213/abf566](https://doi.org/10.3847/2041-8213/abf566)
- Etienne, Z. B., Liu, Y. T., Paschalidis, V., & Shapiro, S. L. 2012a, *Phys. Rev. D*, 85, 064029, doi: [10.1103/PhysRevD.85.064029](https://doi.org/10.1103/PhysRevD.85.064029)
- Etienne, Z. B., Paschalidis, V., Haas, R., Mösta, P., & Shapiro, S. L. 2015, *Class. Quant. Grav.*, 32, 175009, doi: [10.1088/0264-9381/32/17/175009](https://doi.org/10.1088/0264-9381/32/17/175009)
- Etienne, Z. B., Paschalidis, V., & Shapiro, S. L. 2012b, *Phys. Rev. D*, 86, 084026, doi: [10.1103/PhysRevD.86.084026](https://doi.org/10.1103/PhysRevD.86.084026)
- Fernández, R., Foucart, F., Kasen, D., et al. 2017, *Class. Quant. Grav.*, 34, 154001, doi: [10.1088/1361-6382/aa7a77](https://doi.org/10.1088/1361-6382/aa7a77)
- Foucart, F. 2012, *Phys. Rev. D*, 86, 124007, doi: [10.1103/PhysRevD.86.124007](https://doi.org/10.1103/PhysRevD.86.124007)
- Foucart, F., Hinderer, T., & Nisanke, S. 2018, *Phys. Rev. D*, 98, 081501, doi: [10.1103/PhysRevD.98.081501](https://doi.org/10.1103/PhysRevD.98.081501)
- Foucart, F., Kidder, L. E., Pfeiffer, H. P., & Teukolsky, S. A. 2008, *Phys. Rev. D*, 77, 124051, doi: [10.1103/PhysRevD.77.124051](https://doi.org/10.1103/PhysRevD.77.124051)
- Fragione, G. 2021, *Astrophys. J. Lett.*, 923, L2, doi: [10.3847/2041-8213/ac3bcd](https://doi.org/10.3847/2041-8213/ac3bcd)
- Goldreich, P., & Julian, W. H. 1969, *Astrophys. J.*, 157, 869, doi: [10.1086/150119](https://doi.org/10.1086/150119)
- Gommers, R., Virtanen, P., Haberland, M., et al. 2024, *scipy/scipy: SciPy 1.13.1, v1.13.1*, Zenodo, doi: [10.5281/zenodo.11255513](https://doi.org/10.5281/zenodo.11255513)
- Gottlieb, O., Issa, D., Jacquemin-Ide, J., et al. 2023a, *Astrophys. J. Lett.*, 953, L11, doi: [10.3847/2041-8213/acec4a](https://doi.org/10.3847/2041-8213/acec4a)
- Gottlieb, O., et al. 2023b, *Astrophys. J. Lett.*, 954, L21, doi: [10.3847/2041-8213/aceeff](https://doi.org/10.3847/2041-8213/aceeff)
- Grandclement, P. 2006, *Phys. Rev. D*, 74, 124002, doi: [10.1103/PhysRevD.74.124002](https://doi.org/10.1103/PhysRevD.74.124002)
- . 2010, *J. Comput. Phys.*, 229, 3334, doi: [10.1016/j.jcp.2010.01.005](https://doi.org/10.1016/j.jcp.2010.01.005)
- Harris, C. R., Millman, K. J., van der Walt, S. J., et al. 2020, *Nature*, 585, 357, doi: [10.1038/s41586-020-2649-2](https://doi.org/10.1038/s41586-020-2649-2)
- Hayashi, K., Fujibayashi, S., Kiuchi, K., et al. 2022, *Phys. Rev. D*, 106, 023008, doi: [10.1103/PhysRevD.106.023008](https://doi.org/10.1103/PhysRevD.106.023008)
- Hayashi, K., Kiuchi, K., Kyutoku, K., Sekiguchi, Y., & Shibata, M. 2023, *Phys. Rev. D*, 107, 123001, doi: [10.1103/PhysRevD.107.123001](https://doi.org/10.1103/PhysRevD.107.123001)
- Hilditch, D., Bernuzzi, S., Thierfelder, M., et al. 2013, *Phys. Rev. D*, 88, 084057, doi: [10.1103/PhysRevD.88.084057](https://doi.org/10.1103/PhysRevD.88.084057)
- Hoshino, M., Arons, J., Gallant, Y. A., & Langdon, A. B. 1992, *ApJ*, 390, 454, doi: [10.1086/171296](https://doi.org/10.1086/171296)
- Izquierdo, M. R., Bezares, M., Liebling, S., & Palenzuela, C. 2024, *Phys. Rev. D*, 110, 083017, doi: [10.1103/PhysRevD.110.083017](https://doi.org/10.1103/PhysRevD.110.083017)
- Janka, H. T., Eberl, T., Ruffert, M., & Fryer, C. L. 1999, *Astrophys. J. Lett.*, 527, L39, doi: [10.1086/312397](https://doi.org/10.1086/312397)
- Kastaun, W., Kalinani, J. V., & Ciolfi, R. 2021, *Phys. Rev. D*, 103, 023018, doi: [10.1103/PhysRevD.103.023018](https://doi.org/10.1103/PhysRevD.103.023018)
- Kawaguchi, K., Domoto, N., Fujibayashi, S., et al. 2024, *Mon. Not. Roy. Astron. Soc.*, 535, 3711, doi: [10.1093/mnras/stae2594](https://doi.org/10.1093/mnras/stae2594)
- Kawaguchi, K., Kyutoku, K., Shibata, M., & Tanaka, M. 2016, *Astrophys. J.*, 825, 52, doi: [10.3847/0004-637X/825/1/52](https://doi.org/10.3847/0004-637X/825/1/52)
- Kiuchi, K., Sekiguchi, Y., Kyutoku, K., et al. 2015, *Phys. Rev. D*, 92, 064034, doi: [10.1103/PhysRevD.92.064034](https://doi.org/10.1103/PhysRevD.92.064034)



- Komissarov, S. S. 2004a, *Mon. Not. Roy. Astron. Soc.*, 350, 1431, doi: [10.1111/j.1365-2966.2004.07738.x](https://doi.org/10.1111/j.1365-2966.2004.07738.x)
- . 2004b, *Mon. Not. Roy. Astron. Soc.*, 350, 407, doi: [10.1111/j.1365-2966.2004.07446.x](https://doi.org/10.1111/j.1365-2966.2004.07446.x)
- Kyutoku, K., Shibata, M., & Taniguchi, K. 2021, *Living Rev. Rel.*, 24, 5, doi: [10.1007/s41114-021-00033-4](https://doi.org/10.1007/s41114-021-00033-4)
- Lai, D. 2012, *Astrophys. J. Lett.*, 757, L3, doi: [10.1088/2041-8205/757/1/L3](https://doi.org/10.1088/2041-8205/757/1/L3)
- Lattimer, J. M., & Schramm, D. N. 1974, *Astrophys. J. Lett.*, 192, L145, doi: [10.1086/181612](https://doi.org/10.1086/181612)
- Lehner, L., Palenzuela, C., Liebling, S. L., Thompson, C., & Hanna, C. 2012, *Phys. Rev. D*, 86, 104035, doi: [10.1103/PhysRevD.86.104035](https://doi.org/10.1103/PhysRevD.86.104035)
- Levin, J., D’Orazio, D. J., & Garcia-Saenz, S. 2018, *Phys. Rev. D*, 98, 123002, doi: [10.1103/PhysRevD.98.123002](https://doi.org/10.1103/PhysRevD.98.123002)
- Li, L.-X., & Paczynski, B. 1998, *Astrophys. J. Lett.*, 507, L59, doi: [10.1086/311680](https://doi.org/10.1086/311680)
- Loffler, F., et al. 2012, *Class. Quant. Grav.*, 29, 115001, doi: [10.1088/0264-9381/29/11/115001](https://doi.org/10.1088/0264-9381/29/11/115001)
- Londrillo, P., & Del Zanna, L. 2004, *J. Comput. Phys.*, 195, 17, doi: [10.1016/j.jcp.2003.09.016](https://doi.org/10.1016/j.jcp.2003.09.016)
- Lyubarsky, Y. 2014, *Mon. Not. Roy. Astron. Soc.*, 442, 9, doi: [10.1093/mnras/slu046](https://doi.org/10.1093/mnras/slu046)
- Lyubarsky, Y., & Kirk, J. G. 2001, *Astrophys. J.*, 547, 437, doi: [10.1086/318354](https://doi.org/10.1086/318354)
- Lyubarsky, Y. E. 2003, *Mon. Not. Roy. Astron. Soc.*, 339, 765, doi: [10.1046/j.1365-8711.2003.06221.x](https://doi.org/10.1046/j.1365-8711.2003.06221.x)
- Lyutikov, M., & McKinney, J. C. 2011, *Phys. Rev. D*, 84, 084019, doi: [10.1103/PhysRevD.84.084019](https://doi.org/10.1103/PhysRevD.84.084019)
- MacDonald, D., & Thorne, K. S. 1982, *Mon. Not. Roy. Astron. Soc.*, 198, 345
- Martineau, T., Foucart, F., Scheel, M., et al. 2024, <https://arxiv.org/abs/2405.06819>
- McWilliams, S. T., & Levin, J. 2011, *Astrophys. J.*, 742, 90, doi: [10.1088/0004-637X/742/2/90](https://doi.org/10.1088/0004-637X/742/2/90)
- Metzger, B. D. 2020, *Living Rev. Rel.*, 23, 1, doi: [10.1007/s41114-019-0024-0](https://doi.org/10.1007/s41114-019-0024-0)
- Michel, F. C. 1982, *Rev. Mod. Phys.*, 54, 1, doi: [10.1103/RevModPhys.54.1](https://doi.org/10.1103/RevModPhys.54.1)
- Mingarelli, C. M. F., Levin, J., & Lazio, T. J. W. 2015, *Astrophys. J. Lett.*, 814, L20, doi: [10.1088/2041-8205/814/2/L20](https://doi.org/10.1088/2041-8205/814/2/L20)
- Most, E. R., Beloborodov, A. M., & Ripperda, B. 2024a, *Astrophys. J. Lett.*, 974, L12, doi: [10.3847/2041-8213/ad7e1f](https://doi.org/10.3847/2041-8213/ad7e1f)
- Most, E. R., Kim, Y., Chatziioannou, K., & Legred, I. 2024b, *Astrophys. J. Lett.*, 973, L37, doi: [10.3847/2041-8213/ad785c](https://doi.org/10.3847/2041-8213/ad785c)
- Most, E. R., Nathanail, A., & Rezzolla, L. 2018, *Astrophys. J.*, 864, 117, doi: [10.3847/1538-4357/aad6ef](https://doi.org/10.3847/1538-4357/aad6ef)
- Most, E. R., Papenfort, L. J., & Rezzolla, L. 2019, *Monthly Notices of the Royal Astronomical Society*, 490, 3588, doi: [10.1093/mnras/stz2809](https://doi.org/10.1093/mnras/stz2809)
- Most, E. R., Papenfort, L. J., Tootle, S. D., & Rezzolla, L. 2021, *Mon. Not. Roy. Astron. Soc.*, 506, 3511, doi: [10.1093/mnras/stab1824](https://doi.org/10.1093/mnras/stab1824)
- Most, E. R., & Philippov, A. A. 2023, *Astrophys. J. Lett.*, 956, L33, doi: [10.3847/2041-8213/acfdae](https://doi.org/10.3847/2041-8213/acfdae)
- Nathanail, A., & Contopoulos, I. 2014, *Astrophys. J.*, 788, 186, doi: [10.1088/0004-637X/788/2/186](https://doi.org/10.1088/0004-637X/788/2/186)
- Nathanail, A., Most, E. R., & Rezzolla, L. 2017, *Mon. Not. Roy. Astron. Soc.*, 469, L31, doi: [10.1093/mnrasl/slx035](https://doi.org/10.1093/mnrasl/slx035)
- Palenzuela, C. 2013, *Mon. Not. Roy. Astron. Soc.*, 431, 1853, doi: [10.1093/mnras/stt311](https://doi.org/10.1093/mnras/stt311)
- Pan, Z., & Yang, H. 2019, *Phys. Rev. D*, 100, 043025, doi: [10.1103/PhysRevD.100.043025](https://doi.org/10.1103/PhysRevD.100.043025)
- Papenfort, L. J., Tootle, S. D., Grandclément, P., Most, E. R., & Rezzolla, L. 2021, *Phys. Rev. D*, 104, 024057, doi: [10.1103/PhysRevD.104.024057](https://doi.org/10.1103/PhysRevD.104.024057)
- Parfrey, K., Beloborodov, A. M., & Hui, L. 2012, *Mon. Not. Roy. Astron. Soc.*, 423, 1416, doi: [10.1111/j.1365-2966.2012.20969.x](https://doi.org/10.1111/j.1365-2966.2012.20969.x)
- Parfrey, K., & Tchekhovskoy, A. 2017, *Astrophys. J. Lett.*, 851, L34, doi: [10.3847/2041-8213/aa9c85](https://doi.org/10.3847/2041-8213/aa9c85)
- Paschalidis, V., Etienne, Z. B., & Shapiro, S. L. 2013, *Phys. Rev. D*, 88, 021504, doi: [10.1103/PhysRevD.88.021504](https://doi.org/10.1103/PhysRevD.88.021504)
- Paschalidis, V., Ruiz, M., & Shapiro, S. L. 2015, *Astrophys. J. Lett.*, 806, L14, doi: [10.1088/2041-8205/806/1/L14](https://doi.org/10.1088/2041-8205/806/1/L14)
- Penner, A. J., Andersson, N., Jones, D. I., Samuelsson, L., & Hawke, I. 2012, *Astrophys. J. Lett.*, 749, L36, doi: [10.1088/2041-8205/749/2/L36](https://doi.org/10.1088/2041-8205/749/2/L36)
- Petri, J. 2012, *Mon. Not. Roy. Astron. Soc.*, 424, 605, doi: [10.1111/j.1365-2966.2012.21238.x](https://doi.org/10.1111/j.1365-2966.2012.21238.x)
- Philippov, A., Uzdensky, D. A., Spitkovsky, A., & Cerutti, B. 2019, *Astrophys. J. Lett.*, 876, L6, doi: [10.3847/2041-8213/ab1590](https://doi.org/10.3847/2041-8213/ab1590)
- Philippov, A. A., Spitkovsky, A., & Cerutti, B. 2015, *Astrophys. J. Lett.*, 801, L19, doi: [10.1088/2041-8205/801/1/L19](https://doi.org/10.1088/2041-8205/801/1/L19)
- Piro, A. L. 2012, *Astrophys. J.*, 755, 80, doi: [10.1088/0004-637X/755/1/80](https://doi.org/10.1088/0004-637X/755/1/80)
- Poudel, A., Tichy, W., Brüggemann, B., & Dietrich, T. 2020, *Phys. Rev. D*, 102, 104014, doi: [10.1103/PhysRevD.102.104014](https://doi.org/10.1103/PhysRevD.102.104014)
- Ruiz, M., Paschalidis, V., Tsokaros, A., & Shapiro, S. L. 2020, *Phys. Rev. D*, 102, 124077, doi: [10.1103/PhysRevD.102.124077](https://doi.org/10.1103/PhysRevD.102.124077)
- Ruiz, M., Shapiro, S. L., & Tsokaros, A. 2018, *Phys. Rev. D*, 98, 123017, doi: [10.1103/PhysRevD.98.123017](https://doi.org/10.1103/PhysRevD.98.123017)

- Schnetter, E., Hawley, S. H., & Hawke, I. 2004, *Class. Quant. Grav.*, 21, 1465, doi: [10.1088/0264-9381/21/6/014](https://doi.org/10.1088/0264-9381/21/6/014)
- Selvi, S., Porth, O., Ripperda, B., & Sironi, L. 2024, *Astrophys. J. Lett.*, 968, L10, doi: [10.3847/2041-8213/ad4a5b](https://doi.org/10.3847/2041-8213/ad4a5b)
- Shapiro, S. L. 2017, *Phys. Rev. D*, 95, 101303, doi: [10.1103/PhysRevD.95.101303](https://doi.org/10.1103/PhysRevD.95.101303)
- Sironi, L., Plotnikov, I., Näätälä, J., & Beloborodov, A. M. 2021, *Phys. Rev. Lett.*, 127, 035101, doi: [10.1103/PhysRevLett.127.035101](https://doi.org/10.1103/PhysRevLett.127.035101)
- Sironi, L., & Spitkovsky, A. 2014, *Astrophys. J. Lett.*, 783, L21, doi: [10.1088/2041-8205/783/1/L21](https://doi.org/10.1088/2041-8205/783/1/L21)
- Stein, L. C. 2019, *J. Open Source Softw.*, 4, 1683, doi: [10.21105/joss.01683](https://doi.org/10.21105/joss.01683)
- Tacik, N., Foucart, F., Pfeiffer, H. P., et al. 2016, *Class. Quant. Grav.*, 33, 225012, doi: [10.1088/0264-9381/33/22/225012](https://doi.org/10.1088/0264-9381/33/22/225012)
- Tanaka, M., Hotokezaka, K., Kyutoku, K., et al. 2014, *Astrophys. J.*, 780, 31, doi: [10.1088/0004-637X/780/1/31](https://doi.org/10.1088/0004-637X/780/1/31)
- Taniguchi, K., Baumgarte, T. W., Faber, J. A., & Shapiro, S. L. 2007, *Phys. Rev. D*, 75, 084005, doi: [10.1103/PhysRevD.75.084005](https://doi.org/10.1103/PhysRevD.75.084005)
- . 2008, *Phys. Rev. D*, 77, 044003, doi: [10.1103/PhysRevD.77.044003](https://doi.org/10.1103/PhysRevD.77.044003)
- Tchekhovskoy, A., Narayan, R., & McKinney, J. C. 2010, *Astrophys. J.*, 711, 50, doi: [10.1088/0004-637X/711/1/50](https://doi.org/10.1088/0004-637X/711/1/50)
- Tchekhovskoy, A., Philippov, A., & Spitkovsky, A. 2016, *Mon. Not. Roy. Astron. Soc.*, 457, 3384, doi: [10.1093/mnras/stv2869](https://doi.org/10.1093/mnras/stv2869)
- Tchekhovskoy, A., Spitkovsky, A., & Li, J. G. 2013, *Monthly Notices of the Royal Astronomical Society: Letters*, 435, L1, doi: [10.1093/mnrasl/slt076](https://doi.org/10.1093/mnrasl/slt076)
- Teukolsky, S. A. 1972, *Phys. Rev. Lett.*, 29, 1114, doi: [10.1103/PhysRevLett.29.1114](https://doi.org/10.1103/PhysRevLett.29.1114)
- . 1973, *Astrophys. J.*, 185, 635, doi: [10.1086/152444](https://doi.org/10.1086/152444)
- The Matplotlib Development Team. 2024, *Matplotlib: Visualization with Python, v3.9.2*, Zenodo, doi: [10.5281/zenodo.13308876](https://doi.org/10.5281/zenodo.13308876)
- Thornburg, J. 2004, *Class. Quant. Grav.*, 21, 743, doi: [10.1088/0264-9381/21/2/026](https://doi.org/10.1088/0264-9381/21/2/026)
- Tsang, D., Read, J. S., Hinderer, T., Piro, A. L., & Bondarescu, R. 2012, *Phys. Rev. Lett.*, 108, 011102, doi: [10.1103/PhysRevLett.108.011102](https://doi.org/10.1103/PhysRevLett.108.011102)
- Uzdensky, D. A., & Spitkovsky, A. 2014, *Astrophys. J.*, 780, 3, doi: [10.1088/0004-637X/780/1/3](https://doi.org/10.1088/0004-637X/780/1/3)
- Vanthieghem, A., & Levinson, A. 2025, *Phys. Rev. Lett.*, 134, 035201, doi: [10.1103/PhysRevLett.134.035201](https://doi.org/10.1103/PhysRevLett.134.035201)
- Zhang, B. 2019, *Astrophys. J. Lett.*, 873, L9, doi: [10.3847/2041-8213/ab0ae8](https://doi.org/10.3847/2041-8213/ab0ae8)
- Zhong, S.-Q., Dai, Z.-G., & Deng, C.-M. 2019, *Astrophys. J. Lett.*, 883, L19, doi: [10.3847/2041-8213/ab40c5](https://doi.org/10.3847/2041-8213/ab40c5)
- Zlochower, Y., Baker, J. G., Campanelli, M., & Lousto, C. O. 2005, *Phys. Rev. D*, 72, 024021, doi: [10.1103/PhysRevD.72.024021](https://doi.org/10.1103/PhysRevD.72.024021)